

# Birth or burst of financial bubbles: which one is easier to diagnose?

Guilherme Demos <sup>\*†</sup>      Qunzhi Zhang <sup>†</sup>      Didier Sornette <sup>†‡</sup>

## ABSTRACT

Abreu and Brunnermeier (2003) have argued that bubbles are not suppressed by arbitrageurs because they fail to synchronise on the uncertain beginning of the bubble. We propose an indirect quantitative test of this hypothesis and confront it with the alternative according to which bubbles persist due to the difficulty of agreeing on the end of bubbles. We present systematic tests of the precision and reliability with which the beginning  $t_1$  and end  $t_c$  of a bubble can be determined. For this, we use a specific bubble model, the log-periodic power law singularity (LPPLS) model, which represents a bubble as a transient noisy super-exponential price trajectory decorated by accelerated volatility oscillations. Generalising the estimation procedure to endogenise the beginning of the fitting time interval, we quantify the uncertainty on the calibrated  $t_1$  and  $t_c$  (as well as the other model parameters) via the eigenvalues of the Hessian matrix, which characterise the shape of the calibration cost function in the different directions in parameter space, on many synthetic data and four historical bubble cases. We find overwhelming evidence that the beginning of bubbles is much better constrained than their end. Our results are robust over all four empirical bubbles and many synthetic tests, as well as when changing the time of analysis (the “present”) during the development of the bubbles. As a bonus, we find that the two structural parameters of the LPPLS model, the exponent  $m$  controlling the super-exponential growth of price and the angular log-periodic frequency  $\omega$  describing the log-periodic acceleration of volatility, are very “rigid” according to the Hessian matrix analysis, which supports the LPPLS model as a reasonable candidate for describing the generating process of prices during bubbles.

Keywords: Financial bubbles, Time Series Analysis, Numerical Simulation.

JEL classification: C32, C53, G01, G1.

---

\*Corresponding author: [gdemos@ethz.ch](mailto:gdemos@ethz.ch)

<sup>†</sup>ETH Zürich. Rämistrasse 101, 8092 Zürich

<sup>‡</sup>Swiss Finance Institute. Boulevard du Pont-d’Arve 40

# I. Introduction

Financial bubbles and their subsequent crashes provide arguably the most visible departures from well-functional efficient markets. There is an extensive literature (see e.g. the reviews (Kaizoji and Sornette, 2010; Brunnermeier and Oehmke, 2013; Xiong, 2013)) on the causes of bubbles as well as the reasons for bubbles to be sustained over surprising long period of times. One prominent question is: why are not arbitrageurs quelling bubbles in the same way that investment opportunities based on market imperfections tend to be removed by arbitrage? Among many arguments advanced in the literature, we here focus on the one suggested by Abreu and Brunnermeier (2003). In the authors' set-up, market participants become aware about the mispricing developing during the bubble in a disorganised fashion, one after another. Thus, opinions differ about the date when the bubble really started, preventing a coordinated arbitrage that would have put an end to the burgeoning bubble.

We question this view and mechanism. Indeed, from informal private exchanges with a large number of practitioners during massive bubbles (such as the dot-com bubble that terminated in 2000), it appears that the existence of a bubble permeates rather early in the consciousness of professionals. For instance, hedge-funds tend to correctly diagnosed bubbles in their early stages (Gurkaynak, 2008). Think for instance of the famous “irrational exuberance” quip of Federal Reserve chairman, Alan Greenspan, issued on Dec. 5, 1996, more than three years before the bubble finally burst. One could have thought that such a strong statement from such a respected authority (at the time) would have synchronised the attention of arbitrageurs, leading to the demise of this bubble. In fact, after a minor volatility spike lasting no more than a few days following Greenspan's statement, the markets roared unabated to new highs, with the years of 1998 and 1999 enjoying a sky-rocketing cumulative return of more than 1100% for the technology sector. This suggests that bubbles do not persist and flourish because of a lack of general perception of their presence at early times. Rather than shorting the bubble, it is in the interest of investors to “surf” it as long as it lasts (Brunnermeier and Nagel, 2004), given that the gains are so extraordinary that they typically attract less and less sophisticated investors as well as generally less well-informed foreigners, further fuelling the ascent of the bubble (Shleifer, 2000; Sornette, 2003). Moreover, it often happens that value investors opportunistically transform into momentum followers during bubble regimes.

Rather than the beginning of bubbles, we argue that it is their ends that are devilishly difficult to forecast with any useful accuracy. As Keynes famously commented: “The market can stay irrational longer than you can stay solvent.” And Greenspan's statement mentioned above also illustrates the discrepancy between an early diagnostic and the much delayed con-

clusion of the bubble. The contribution of the present article is to propose a methodology to quantify these intuitions. We put numbers on how precise can be the early diagnostic of a nucleating bubble and the estimation of its lifetime. For this, we use the log-periodic power law singularity (LPPLS) model (Johansen, Ledoit, and Sornette, 2000; Sornette, 2003) to represent bubble regimes. We endogenize  $t_1$  as a parameter to calibrate and estimate the LPPLS model on synthetic time series generated by the LPPLS model with noise and on four historical bubble cases. In order to determine the uncertainties of the calibrated parameters, we calculate the eigenvalues and eigenvectors of the Fisher Information Matrix defined from the cost function of the calibration exercise, following Transtrum, Machta, and Sethna (2011) and Machta, Chachra, Transtrum, and Sethna (2013). Comparing the eigenvalues and the parameters that contribute to the corresponding eigenvalues, we can estimate the “rigid” parameters versus the “sloppy” ones, the later being characterised by very small eigenvalues so that the cost function is essentially insensitive to their specific values, making them impossible to determine precisely. We find that the eigenvalues of the Hessian matrix approximated at the best-fit parameters whose eigenvectors are dominated by  $t_1$  tend to be three orders of magnitude larger than those controlled by  $t_c$ . As a rough estimate, this implies that the errors on  $t_c$  are about 30 times larger than on  $t_1$ . The determination of the end of the bubble is thus much more difficult than its beginning. This suggests that the lack of knowledge regarding the end of the bubble  $t_c$  should play a more important role on asset price inflation than the lack of agents consensus about  $t_1$ .

The article is structured as follows. Section II presents the Log-Periodic Power-Law Singularity model (Johansen et al., 2000) alongside with an initial result of the sloppy-rigid analysis performed on synthetic data. We then extend the application of the method to real world data in Sec. III and conclude in Section IV.

## II. The Log-Periodic Power-Law Singularity (LPPLS) model

### A. Brief review of the literature on bubbles

The weak *efficient-market-hypothesis* stresses that prices should reflect all available information at a given time (Samuelson, 1965) while any mispricing should be promptly arbitrated by market makers. In reality, many anomalies seem to persist, the bubble phenomenon being arguably the prominent one. Financial bubbles are often considered a product of coordinating interactions at the microscopic level between economic agents, leading to the observed price trajectory of an asset to decouple from its underlying fundamental value (Kindleberger,

1978; Sornette, 2003). Why do bubbles start and why they persist are subjects of much controversy (Kindleberger, 1978; Sornette, 2014; Xiong, 2013).

Minsky and Hyman (1974) suggested the importance of loose monetary policy in enhancing the price decoupling during bubbles. Innovations, both financial and technological, also tend to be associated with beginnings of bubbles (Shiller, 1981; Kindleberger, 1978). Moreover, the task of correctly pricing the fundamental value of a given firm or asset involves much uncertainty, due to inherent sensitivity of the method of discounting future dividends or earnings through time (Gurkaynak, 2008).

Financial bubbles were shown to be persistent even in the presence of rational expectation agents (Blanchard and Watson, 1982). The behavioral feedback-loop theory for example holds that higher present observable prices lead to higher expected price appreciation (Barberis, Shleifer, and Vishny, 1998; Shiller, 2000). This resembles the resale option theory (Harrison and Kreps, 1978). In this framework, rational agents are willing to pay more than their own expectation of the asset fundamental value because they expect to re-sell the asset in the future to a more optimistic agent, for a higher price. Hüsler, Sornette, and Hommes (2012) test these ideas quantitatively in a set of bubble experiments.

## *B. Presentation of the model*

Building on this idea of positive feedbacks by imitation, the JLS model proposed by Johansen et al. (2000) and its extensions includes as a key ingredient the role played by herding behaviour in the formation of bubbles. Considering bubbles as a transient phenomena, the existence of positive feedbacks between value investors and noise traders create a super-exponential growth of the price, decorated by deviations around the price growth in the form of oscillations that are periodic in the logarithm of the time to the burst of the bubble. When imitation reaches a certain threshold, the higher demand for the asset leads to the observable price to increase, bootstrapping on itself, and the market is governed by sentiment rather than some real underlying value (Sornette and Cauwels, 2015). This process is intrinsically unsustainable and the mispricing ends at a critical time  $t_c$ , either smoothly into another regime or abruptly (crash). In short, in this set-up (as well as the one discussed above (Abreu and Brunnermeier, 2003)), it is assumed that agents are fully aware of the mispricing.

In a bubble regime, the observed price trajectory of a given asset decouples from its intrinsic fundamental value (Kindleberger, 1978; Sornette, 2003). For a given fundamental value, the JLS model (Johansen et al., 2000) assumes that the logarithm of the observable

asset price  $p(t)$  follows

$$\frac{d(p)}{p} = \mu(t)dt + \sigma(t)dW - kdj, \quad (1)$$

where  $\mu(t)$  is the expected return,  $\sigma(t)$  is the volatility,  $dW$  is the infinitesimal increment of a standard Wiener process and  $dj$  represents a discontinuous jump such that  $j = n$  before and  $j = n + 1$  after a crash occurs (where  $n$  is an integer). The parameter  $k$  quantifies the amplitude of a possible crash.

Two types of agents are considered: the first group consists in traders with rational expectations (Blanchard and Watson, 1982), while the second one is characterized by noise traders with herding behaviour. The collective behaviour of the latter class of traders can destabilise asset prices. Johansen et al. (2000) propose that their behaviour can be mimicked by writing the *crash hazard rate* under the following form

$$h(t) = \alpha(t_c - t)^{m-1}(1 + \beta \cos(\omega \ln(t_c - t) - \phi')), \quad (2)$$

where  $\alpha, \beta, \omega$  and  $t_c$  are parameters. Eq. (2) tells us that the risk of a crash resulting from herding behaviour is a sum of a power law singularity ( $\alpha(t_c - t)^{m-1}$ ), which is decorated by large scale amplitude oscillations that are periodic in the logarithm of the time to the singularity (or critical time)  $t_c$ . The power law singularity embodies the positive feedback mechanism associated with the herding behaviour of noise traders. The log-periodic oscillations represent the tension and competition between the two types of agents that tend to create deviations around the faster-than-exponential price growth as the market approaches a finite-time-singularity at  $t_c$ .

The no-arbitrage condition imposes that the excess return  $\mu(t)$  during a bubble phase is proportional to the crash hazard rate given by Eq. (2). Indeed, setting  $E[dp] = 0$ , and assuming that no-crash has yet occurred ( $dj = 0$ ), this yields  $\mu = kh(t)$ , since  $E[dj] = h(t)dt$  by definition of  $h(t)$ . By integration, we obtain the expected trajectory of the price logarithm during a bubbly trajectory, conditional on the crash not yet happening, as

$$E[\ln p(t)] = A + B|t_c - t|^m + C|t_c - t|^m \cos(\omega \ln |t_c - t| - \phi) , \quad (3)$$

with  $B = -k\alpha/m$  and  $C = -k\alpha\beta/\sqrt{m^2 + \omega^2}$ . Note that the formula extends the price dynamics beyond  $t_c$  by replacing  $t_c - t$  by  $|t_c - t|$ , which corresponds to assuming a symmetric behavior of the average of the log-price around the singularity at  $t_c$ .

Bubble regimes are in general characterized by  $0 < m < 1$  and  $B < 0$ . The first condition  $m < 1$  writes that a singularity exists (the momentum of the expected log-price diverges at

$t_c$  for  $m < 1$ ), while  $m > 0$  ensures that the price remains finite at the critical time  $t_c$ . The second condition  $B < 0$  expresses that the price is indeed growing super-exponentially towards  $t_c$  (for  $0 < m < 1$ ),

### C. Estimating the model

Filimonov and Sornette (2013) re-wrote expression (3) by expanding the term  $C \cos[.]$  to replace the two parameters  $C$  and  $\phi$  by two linear parameters  $C_1 = C \cos \phi$  and  $C_2 = C \sin \phi$ . This representation reduces the complexity of the calibration of the LPPLS model through the reduction of the number of nonlinear (NL) parameters from 4 ( $m, \omega, t_c, \phi$ ) to 3 ( $m, \omega, t_c$ ), while augmenting the set of linear parameters to 4 ( $A, B, C_1, C_2$ ). In the present article, each fit was performed using the Levenberg-Marquardt algorithm (Marquardt, 1962), with starting values for the nonlinear parameters obtained from a previous Nelder-Mead Simplex search method. Appendix A summarises the two-step procedure used to determine first the 4 slaved linear parameters and then the 3 nonlinear parameters.

Previous calibrations of the JLS model have further shown the value of additional constraints imposed on the nonlinear parameters in order to remove spurious calibrations (false positive identification of bubbles) (Sornette and Johansen, 2001; Johansen and Sornette, 2010; Jiang, Zhou, Sornette, Woodard, Bastiaensen, and Cauwels, 2010; Geraskin and Fantazzini, 2011).

1. **exponent**  $0.1 < m < 0.9$ : This more stringent constraint than the one ( $0 < m < 1$ ) discussed above improves the power of discriminating bubbles by removing calibrations that select parameters too close from the bounds.
2. **angular log-periodic frequency**  $6 < \omega < 13$ : This condition ensures that the preferred scaling ratio  $:= e^{\frac{2\pi}{\omega}}$  of the log-periodicity (Sornette, 1998) is of the order of 2, as suggested by general theoretical arguments (Saleur and Sornette, 1996).
3. **Search interval for  $t_c$  given by**  $t_2 + 1 < t_c < t_2 + \eta ||t_2 - t_1||$ , where time is in units of days.  $[t_1, t_2]$  is the time window in which the calibration is performed. One can think of  $t_2$  as the “present” time, in the sense that it is the latest time at which information is used to calibrate the model. The beginning  $t_1$  of the fitting interval sets the time scale  $t_2 - t_1$  of the analysis. The factor  $\eta$  is of the order of 1, often chosen about 1/3 or 1/2 to ensure that the remaining bubble lifetime is within an horizon of predictability estimated to scale proportionally to the width of the analysing window.
4. **“Damping” condition**: Within the RE bubble framework used by the JLS model, the crash hazard rate is found to be proportional to the expected return during the bubble, conditional on the fact that the bubble has not yet burst. Since the crash hazard rate

is by definition a non-negative quantity, this imposes that the expected return during the bubble should be non-negative. This can be shown to impose that condition  $D \geq 1$  where  $D := \frac{|B|m}{\omega\sqrt{C_1^2+C_2^2}}$  (Graf v. Bothmer and Meister, 2003). Intuitively, the amplitude of the log-periodic oscillations should be not too large compared with the acceleration of the price so that their combination ensures the non-negativity of the expected return at all times during the bubble. Of course, the realized stochastic return can be negative. It is only its expectation that should be non-negative.

5. **Number of oscillations:** The number of oscillations (half-periods) of the log-periodic component is given by  $O := \frac{\omega}{\pi} \ln \left( \frac{t_c - t_1}{t_c - t_2} \right)$ . Huang, Johansen, Lee, Saleur, and Sornette (2000) showed that a minimum number of oscillations is needed to distinguish a genuine log-periodic signal from one that could be generated by noise. In the present implementation, we qualify a fit only if  $O \geq 2.5$ .
6. **residuals  $r \sim \text{AR}(1)$ :** Lin, Ren, and Sornette (2014) have emphasised the need for the residuals of the LPPLS calibration to be mean-reverting in order for the calibration of the log-price by the LPPLS model (3) to be consistent. Hence, we test for the mean-reverting (O-U) property of the residuals of the fit, using both the standard unit-root Augmented Dickey-Fuller and Phillips-Perron tests.

#### D. Expanded parameter space to endogenize $t_1$

Because the goal of the present article is to determine which of the beginning or the end of a bubble is best estimated, we propose to endogenize the search for the beginning of the bubble in the calibration of the parameters. For this, we define the beginning of the bubble as the ‘best’ beginning time  $t_1$  of the interval  $[t_1, t_2]$  in which the calibration is performed, ‘best’ in the sense of minimising an appropriate scaled goodness of fit. This leads to an expanded nonlinear parameter set  $\Phi = \{m, \omega, t_c, t_1\}$ . The  $L^2$  cost function to minimise generalises expression (12) in Appendix A to make explicit the beginning time  $t_1$  of the time interval in the optimisation problem. In order to make different windows  $[t_1, t_2]$  comparable, we normalise the sum of squares of the residuals by the number  $t_2 - t_1$  of points in the sum (Tsay, 2010)

$$\chi^2(\Phi) := F_2(m, \omega, t_c, t_1) = \frac{1}{t_2 - t_1} \sum_{i=t_1}^{t_2} r_i(\Phi)^2, \quad \text{with } r_i(\Phi) = y(t)_i - flppl(\Phi, t)_i, \quad (4)$$

where  $flppl(\Phi, t)_i$  is defined by expression (8) in Appendix A. The calibration of the parameters  $\Phi$  is performed by following the same procedure as explained in Appendix A, which is explicated in Appendix B.



### E. Hessian matrix, its eigenvalues and eigenvectors quantifying rigidity vs. sloppiness

Since we are interested in the *relative parameter variations* and their corresponding impact upon  $\chi^2$ , each parameter  $[m, \omega, t_c, t_1] \in \Phi$  was standardized using

$$\tilde{\Phi}_i = \frac{\Phi_i - \langle \Phi_i \rangle}{\sigma(\Phi_i)}, \quad (5)$$

where  $\langle \Phi_i \rangle$  and  $\sigma(\Phi_i)$  denotes respectively the median and the standard deviation of parameter  $i$  within its respective theoretical bound (see conditions 1-3 in Sec. II.C). This transformation ensures that the mean of  $\tilde{\Phi}_i$  is 0 and its standard deviation is equal to 1 for all 4 nonlinear parameters. This allows us to compare their sloppiness (Brown and Sethna, 2003) based on a study of the Hessian matrix given by Eq. (26) in Appendix B.

Once the optimal parameter set  $\Phi^*$  is obtained and after standardisation, we computed the Jacobian  $J(\Phi^*)$  defined by (21) using Eq. (26) in Appendix B. For small residuals  $\mathbf{r}$ , the Hessian matrix about the best-fit is then approximated by Eq. (24) using  $\mathbf{J}^\top \mathbf{J}$ . Recall that the Hessian matrix provides a quantification of the shape of the cost function in parameter space. The spectrum of eigenvalues  $\{\lambda_i\}$  and their associated eigenvectors  $\{\vec{v}_i\}$  of the Hessian matrix embody the information on the directions in parameter space that are best determined. Large eigenvalues correspond to rigid parameters (or combination of parameters), i.e., for which a small variation entails a relatively large change of the cost function. In contrast, small eigenvalues identify the “sloppy” parameters (or combination of parameters) that are poorly constrained, so that a rather large variation of their value does not change much the cost function. Geometrically, one can picture the cost function as made of wide valleys with elongated flat profiles along the eigenvectors with small eigenvalues, and of sharp narrow valleys along the eigenvectors with large eigenvalues. If, as we find below, a given eigenvector is dominated by one of the parameters, its corresponding eigenvalue determines the rigidity vs. sloppiness of that parameter (rigid if the eigenvalue is relatively large and sloppy if small).

In practice, fits whose spread between the largest and the smallest eigenvalue surpasses roughly three orders of magnitude are considered *sloppy* (Machta et al., 2013). Generally, this results from a near degenerate Hessian matrix (see Eq. (22)), where changes in a given parameter do not lead to an increase of the cost function since this change can be compensated by that of another parameter along the sloppy direction. It is important to keep in mind, however, that even though large parameter uncertainty does in general exist, the macroscopic behavior of the system is not necessarily compromised (Bak, Tang,



and Wiesenfeld, 1988; Transtrum and Sethna, 2012), given that predictions rely on rigid directions of the model.

### F. Construction of synthetic LPPLS bubbles

To gain insight about the parameter structure of the extended LPPLS model and thus establish a solid background to our empirical analysis, we generate synthetic price time series. The synthetic price time series (a realisation is depicted in Fig. 1(a)) are obtained by using formula (3) with parameters given by the best LPPLS fit within the window  $w \in [t_1 = \text{Jan. 1981}; t_2 = \text{Aug. 1987}]$  of the bubble that ended with the Black Monday 19 Oct. 1987 crash. These parameters are ( $m = 0.44$ ,  $\omega = 6.5$ ,  $C_1 = -0.0001$ ,  $C_2 = 0.0005$ ,  $A = 1.8259$ ,  $B = -0.0094$ ,  $t_c = 1194$ ). To the deterministic component describing the expected log-price given by expression (3) and denoted by  $flppls(\phi, t)$  (as in Appendix A, see expression (8)), we add a stochastic element according to

$$\ln[P(t)] = flppls(\phi, t) \left( \frac{1 + \varepsilon(t) \sigma}{\max(lppls(t))} \right), \quad (6)$$

where  $t = [1, \dots, N = 1100]$ . This corresponds to multiplicative (or proportional) noise term with  $\varepsilon \sim \mathcal{N}(\mu, \sigma^2)$  and  $\sigma = 0.1$ ,  $\mu = 0$ . The black stochastic line in Fig. 1(a) represent  $\ln[P(t)]$  given by (6).

For each synthetic bubble price time series, we calibrated it with Eq. (3) by minimizing expression (4) in windows  $[t_1, t_2]$ , scanning  $t_2$  from 1981/01/01 to  $t_2 = 1987/08/12$ , with  $t_1$  varying from  $t_1 = \text{Jan. 1981}$  up to 60 business days before  $t_2$ , i.e. up to  $t_{1,max} = t_2 - 60$  for each fixed  $t_2$ . Then, the Hessian matrix was approximated about the best-fit parameters for each  $t_1$  and its corresponding eigenvalues were calculated.

### G. Sloppiness and Rigidity of $t_c$ vs. $t_1$ using synthetic price time series

We now extend the initial sloppy-rigid analysis performed in the LPPLS framework by Bree, Challet, and Peirano (2013), in order to test which one of the two parameters, beginning  $t_1$  or the forecasted end  $\hat{t}_c$  of a bubble, is the most sloppy, i.e., has the largest uncertainty.

For illustration of the typical situation found in these synthetic tests (to be extended below), we perform the calibration of synthetic noisy price time series in the full window shown in Fig. 1(a) corresponding to  $[t_1 = \text{Jan. 1981}; t_2 = \text{Aug. 1987}]$  (represented as  $[Date = 1 : Date = 1100]$ ). For a given realisation, we calculate the Hessian matrix and the corresponding eigenvalues and eigenvectors. We consider both the case of a fixed  $t_1$  with cost

function (12) (bottom rows of table I) and of the extended cost function (4) endogenizing  $t_1$  as a parameter to be determined (top rows of table I). The entries of the two Hessian matrices are given in the columns on the left of the table and their eigenvalues in the central column  $\lambda$ .

Note first that the smallest eigenvalue is of the order  $10^{-8}$  times the largest eigenvalue, exemplifying the sloppy nature of the calibration. In the right columns of the table, the components of the corresponding eigenvectors show that the largest eigenvalue is mainly determined by parameter  $m$ , the second largest one is mainly controlled by parameter  $\omega$  and the smallest eigenvalue is always mainly associated with parameter  $t_c$ , confirming that the end of the bubble is very difficult to determine as the cost function is essentially degenerate in the direction of  $t_c$  in parameter space.

Interestingly, for the extended cost function, one can observe that the eigenvalue dominated by parameter  $t_1$ , while being smaller than the two others associated with  $m$  and  $\omega$ , is approximately 4000 times larger than the eigenvalue describing the sloppiness of  $t_c$ . This is a first illustration that  $t_1$  is much more rigidly determined (or depending on taste much less sloppy) than  $t_c$ . Indeed, using a geometrical intuitive interpretation, contour lines of the cost function form approximate ellipses whose axis lengths are inversely proportional to the square root of their corresponding eigenvalue  $\lambda$  (axis length  $\simeq 1/\lambda^{\frac{1}{2}}$ ). Thus a factor 4000 translates into a size of the axis along  $t_c$  about 60 times larger than the axis along  $t_1$ . In other words, in this illustration, the uncertainty on  $t_1$  is about 60 times smaller than on  $t_c$ .

Does this result hold for other time windows and in particular far from the end of the bubble? To investigate this question, we perform the same exercise of calibrating the LPPLS formula in windows  $[t_1, t_2]$ , varying  $t_1$  from  $Date = 1$  (about four years before the crash) to  $Date = 1040$  days (close to the crash). The blue circles and red squares in Fig (1(a)) display the obtained normalised eigenvalues  $\lambda_3$  and  $\lambda_4$  in logarithm scale, associated respectively to  $t_1$  and  $t_c$ . By ‘normalised’, we mean that each eigenvalue obtained for a given calibration is divided by the largest one (i.e. that associated mainly with  $m$ ). By repeating this process 100 times, confidence bounds for the eigenvalues for each  $t_1$  can be determined and are depicted by the error bars. Figure 1 confirms that  $t_1$  is always more rigid than  $t_c$  by far at all times  $t_2$ . It is particularly noteworthy that the situation for  $t_c$  does not improve in absolute terms or relative to  $t_1$  even when getting closer and closer to the true end of the bubble: while the determination of the beginning  $t_1$  of the bubble can be reasonably estimated, that of the end  $t_c$  remains much more elusive. One can also observe a rather stable behavior of these two eigenvalues when  $t_1$  spans 1 to 600 days. Interestingly, the vast majority of fits performed during this time window correctly qualify the underlying time series as being in a bubble regime.

For Date =  $t_1 > 600$ , one can observe a fast drop of the eigenvalues associated with  $t_1$  and  $t_c$ , which can be explained by the average negative curvature of the log-price associated with the first large log-periodic oscillation. This negative curvature confounds the information on the existence of the supposed super-exponential bubble and thus on the determination of both its beginning ( $t_1$ ) and its end ( $t_c$ ). When the average curvature of the log-price becomes positive again, one can observe a jump of the two eigenvalues upward, back to almost the same level as before the first jump down. This is followed by a further decrease of the eigenvalues as  $t_1$  approaches too close to the true  $t_c$ .

The lower part of panel (a) of Fig. 1 checks that the two smallest eigenvalues  $\lambda_3$  and  $\lambda_4$  are indeed mostly representing respectively the directions along  $t_1$  and  $t_c$  of the cost function. To quantify that this is the case, let us denote  $\vec{v}(t_{1,\lambda_3})$  the component on  $t_1$  of the third vector associated with the third largest eigenvalue  $\lambda_3$ . Similarly, let  $\vec{v}(t_{c,\lambda_4})$  be the component on  $t_c$  of the fourth vector associated with the smallest eigenvalue  $\lambda_4$ . Analogously,  $\vec{v}(\Phi_j, \lambda_i)$  is the component on parameter  $\Phi_j$  of the eigenvector associated with the eigenvalue  $\lambda_i$ . Let us introduce the weights

$$C_{t_1, \lambda_3} = \frac{|\vec{v}(t_{1,\lambda_3})|}{\sum_{j=1}^4 \sqrt{\vec{v}(\Phi_j, \lambda_3)^2}}, \quad C_{t_c, \lambda_4} = \frac{|\vec{v}(t_{c,\lambda_4})|}{\sum_{j=1}^4 \sqrt{\vec{v}(\Phi_j, \lambda_4)^2}}. \quad (7)$$

These weights  $C_{t_1, \lambda_3}$  and  $C_{t_c, \lambda_4}$  are shown in the lower part of panel (a) of Fig. 1 and confirm that the relative contributions of parameter  $t_1$  (resp.  $t_c$ ) in the eigenvector along  $\lambda_3$  (resp.  $\lambda_4$ ) is never smaller than  $\approx 90\%$  (respec.  $99\%$ ).

The distributions of the normalized eigenvalues  $\lambda_2/\lambda_1$ ,  $\lambda_3/\lambda_1$  and  $\lambda_4/\lambda_1$  over the ensemble of  $t_1$  values for a fixed  $t_2$  and a single log-price realisation are depicted in Fig. 1(b). The dashed lines show the mean values of the three distributions. This confirms that  $t_1$  is much more rigid than  $t_c$  across all windows and that the hierarchy from rigid to sloppy is from  $m, \omega, t_1$  to  $t_c$ .

For the fixed Date  $t_2 = 150$ , figures 1(c)-1(h) show cross-sections of the cost function for parameters  $m$ ,  $\omega$ ,  $t_1$  and  $t_c$ . The shape of the cost function exhibits the valley patterns whose relative extensions in different directions are quantified by the eigenvalues, as discussed above. Figs. 1(c) and 1(d) show that, for parameters  $m$  vs.  $\omega$  and  $m$  vs.  $t_c$ , the elliptic contour lines close to the cost function minimum are aligned approximately along the parameter axes. In contrast, for the parameter space of  $t_c$  vs.  $\omega$ , the largest eigen-direction is along the diagonal direction. This feature expresses the fact that parameters  $\omega$  and  $t_c$  are strongly correlated in the calibration process. In practice, this implies the existence of several values of  $t_c$  that are consistent with a low cost value, given that parameter  $\omega$  (see Fig 1(e)) can be tuned to take this variation into account. Thus, this interdependency should be considered

properly when constructing confidence intervals for  $\omega$  and  $t_c$ .

For robustness, a sensitive analysis was performed around the best solutions of  $\hat{t}_1^*$  and  $\hat{t}_c^*$ . By taking into account the sample size, the box-plot shown in fig. 1(a) gives the corresponding  $\chi^2$  variation when each  $t_1 \in \hat{t}_1^*$  and  $t_c \in \hat{t}_c^*$  are used as input parameters in Eq. 4. Results confirm that changes in  $t_1$  leads to cost variations ranging from -4% to 4% while changes in  $\hat{t}_c^*$  yields a negligible change. This is due to the compensation provided by the correlation between  $\omega$  and the critical time parameter (see Fig. 1(e)) previously mentioned.

Finally, the coloured *pdf's* in Fig 1(a) were constructed over the qualified fits (according to the filtering criteria of Sec II.C) of the ensemble of noise realisations for a fixed  $\bar{t}_2$ . The fact that the  $pdf(\hat{t}_1^*)$  is wider than  $pdf(\hat{t}_c^*)$  is not contradicting our key result that  $t_1$  is much better estimated than  $t_c$  *for a specific realisation*. In a real life situation, one can only analyse one single realisation given by history. In contrast, the coloured *pdf's* in Fig 1(a) provide artifactual information, i.e. on an ensemble of statistically equivalent price trajectories differentiated only by the different realisations of the noise process. The fact that the  $pdf(\hat{t}_1^*)$  is wider than  $pdf(\hat{t}_c^*)$  thus inform us that there is more variability of  $t_1$  than  $t_c$  from one realisation to another one. This results from the structure of log-periodicity, with slow oscillations at early times and fast oscillations close to  $t_c$ .

### III. Empirical tests

#### A. Data: four historical bubbles

In this section, we perform the same procedure as described in the previous section on real bubble events. Scanning a time interval extending from several years before until the burst of each bubble, we first determine the time  $\bar{t}_2$  at which the price reached its maximum before the crash starts to develop. We fix this time as the end of our time window of analysis. Obviously, this procedure is not correct for forecasts as it uses future information (the fact that  $\bar{t}_2$  was the maximum before the crash) but is useful to reduce the number of degrees of freedom for our purposes. Further down, we drop this assumption and incorporate random  $t_2$ 's into the analysis (see III.C). For this fixed  $\bar{t}_2$ , our fitting windows scan  $t_1$  using daily observations ranging from some  $t_{1,i=1}$  until  $t_{1,\bar{t}_2-60}$ , where the unit of time is one day, which are used as input for the  $t_1$  parameter during the calibration process (4).

We have chosen a representative set of four well-known bubbles, augmented by the synthetic bubbles given by (6) for comparison.

- **Shanghai Stock Exchange Composite Index bubble ending in October 2007 (SSEC):**

This bubble has been documented and studied by [Jiang et al. \(2010\)](#). For  $\bar{t}_2 = 10 \text{ Oct } 2007$ , our fitting windows scan  $t_1$  using daily observations ranging from  $t_{1,i=1} = 2005/01/01$  until  $t_{1,\bar{t}_2-60} = 2007/08/10$ . Converting from calendar time to time counted in unit of days, we have  $t_{1,i=1} = 1$  and  $\bar{t}_2 = 676$ . Thus, there are 616 different possible windows for the fixed end time  $\bar{t}_2 = 676$ , the different windows corresponding to the different  $t_{1,1} = 1, t_{1,2} = 2, \dots, t_{1,\bar{t}_2-60} = 616$ , which are used as input for the  $t_1$  parameter during the calibration process (4). Note that the smallest (resp. largest) window has a duration of 60 (resp. 676) days.

- **S&P500 Index bubble ending in October 2007 (SP):**

This bubble has been documented and studied in ([Sornette and Woodard, 2010](#); [Sornette and Cauwels, 2014, 2015](#)). The same procedure as described for the previous bubble was applied to the *S&P500*. With the choice  $\bar{t}_2 = \text{Jul.15 } 2007$ , our fitting windows scan  $t_1$  using daily observations ranging from  $t_{1,i=1} = 2002/01/01$  to  $t_{1,\bar{t}_2-60} = 2007/05/01$ . This yields a total of  $N = 1332$  different possible values of  $t_1$  over which to perform the calibration process (4).

- **S&P500 Index bubble ending on Black Monday, October 19, 1987 (BM):**

This bubble has been documented and studied by [Sornette, Johansen, and Bouchaud \(1995\)](#). Choosing  $\bar{t}_2 = \text{Aug.15 } 1987$ , our fitting windows scan  $t_1$  using daily observations ranging from  $t_{1,i=1} = 1981/01/01$  until  $t_{1,\bar{t}_2-60} = 1987/06/12$ . This yields a total of  $N = 1674$  different possible values of  $t_1$  over which to perform the calibration process (4).

- **Bovespa Index bubble ending in December 2003:**

Choosing  $\bar{t}_2 = \text{Dec. } 2003$ , our fitting windows scan  $t_1$  using daily observations ranging from  $t_{1,i=1} = 2002/01/01$  until  $t_{1,\bar{t}_2-60} = 2003/10/01$ . This yields a total of  $N = 417$  different possible values of  $t_1$  over which to perform the calibration process (4).

For each of these four empirical time series, the corresponding residuals  $r(t)$ 's defined in (4) are obtained for each window  $[t_1, \bar{t}_2]$  and the set of their probability density functions (pdf) obtained when scanning  $t_1$  are shown in Fig. 7 of the Supplementary Materials. Except from moments where fits are not qualified, the residuals are well-behaved and are approximately normally distributed.

### B. Analysis of the cost function $\chi^2(\Phi)$ and its Hessian

For the four empirical bubbles, figure 2 presents the pdf's of the normalized eigenvalues  $\lambda_2/\lambda_1$ ,  $\lambda_3/\lambda_1$  and  $\lambda_4/\lambda_1$  of the Hessian matrix  $H|_{(\Phi)}^*$ , over the ensemble of  $t_1$  values scanned in the analysis. As in table I obtained for a synthetic bubble, we find almost systematically that the largest eigenvalue is dominated by parameter  $m$ . The exception is the *SSEC* Index, where the largest eigenvalue  $\lambda_1$  corresponds to  $\omega$  and the second largest  $\lambda_2$  to  $m$ . The colors of the pdf's encode the parameter that dominates its corresponding eigenvalue: green for  $m$ , grey for  $\omega$ , blue for  $t_1$  and red for  $t_c$ . One can observe that the normalized  $\lambda_3$  (blue pdf) associated predominantly with  $t_1$  are systematically much larger than the values of the normalized  $\lambda_4$  (red pdf) associated predominantly with  $t_c$ . This confirms for these four empirical bubbles the conclusion obtained in the synthetic tests. Moreover, we find that, for the *SSEC* and *S&P500 (BM)* bubbles, more than 80% of the windows give a normalized  $\lambda_2 > 10^{-3}$ , allowing us to conclude that  $\omega$  (and a fortiori  $m$ ) is a relatively rigid parameter. For the two other bubbles,  $\lambda_2 > 10^{-3}$  for just about 50% of the time windows.

Overall, the eigenvalues  $\lambda_i^E \equiv \lambda_i$ , for  $i = [m, \omega, t_1, t_c]$  exhibit a mixture of jumps intercalated with intervals of stable downward trends as the window length shrinks and  $t_1$  approaches  $t_2$  (see figure 8 of the Supplementary Materials.). When using the original cost function (12), the same pattern for the contribution of the parameters to the eigenvectors is observed (see Figure 10 in the Supplementary Materials) as well as the same behaviour of the eigenvalues as a function of  $t_1$  (see Fig 9). The overall sloppiness does not change substantially when using the extended cost function  $F_2$  (expression (4)) instead of  $F_1$  (see definition (13)).

Figure 3 displays three two-dimensional cross-sections of the cost function  $\chi^2(\Phi^*)$  for the four empirical bubbles along the three different pairs of structural parameters  $(m, \omega)$ ,  $(t_c, m)$  and  $(t_c, \omega)$ . The corresponding values of the Hessian matrix, eigenvectors and eigenvalues are summarised in Table II. Under the same conditions, Table III gives the values of the Hessian matrix, of the eigenvalues  $\lambda$  and associated eigenvectors  $\vec{v}$  using the original cost function (13) without  $t_1$ . Applying the standard unit-root Augmented Dickey-Fuller and Phillips-Perron tests to the residuals of the best fits confirms that they are mean-reversing, in agreement with the condition proposed by Lin et al. (2014) (see Table IV and figure 7 in the Supplementary Materials). Figure 3 shows the same ellipse-shaped structure as obtained previously in our synthetic tests described in section II.F and the same order of the importance of the parameters  $m, \omega, t_1$  and  $t_c$  associated respectively from the largest eigenvalue to the smallest one. This structure is also robust when using the LPPLS cost function without  $t_1$  as a parameter to calibrate (see Table III).

The dependence of the cost function  $\chi^2(\Phi)$  for the same four studied empirical bubbles

along the three different pairs of parameters  $(t_1, m)$ ,  $(t_1, \omega)$  and  $(t_1, t_c)$  is shown in fig. 4. One can observe a much more complicated landscape than in figure 3 with multiple local minima associated with the introduction of the parameter  $t_1$ . Figure 4 demonstrates that the normalised cost function exhibits an overall decrease as  $t_1$  increases, because the calibration has a smaller number of degrees of freedom to explain for smaller  $t_2 - t_1$ . This tends to bias the estimation of  $t_1$  upward, i.e., to underestimate the true duration of the bubble. Figures 4(c), 4(f), 4(i) and 4(l) exemplify that  $t_c$  has very little impact on the value of  $\chi^2(\Phi)$  once  $t_1$  is given. In other words, one can really visualise here the sloppiness of  $t_c$  compared with the relatively much larger rigidity of  $t_1$ . This feature is absent for the pairs  $(t_1, m)$  and  $(t_1, \omega)$ , as small changes in  $m$  and  $\omega$  often lead to significant variations of the cost function, in agreement with the information contained in the corresponding eigenvalues. One can also observe that, for certain values of  $t_1$ , the cost function exhibits clear minima as a function of  $t_c$ , supporting previous claims that the end of financial bubbles may be predictable only at certain time intervals, i.e., in “pockets of predictability” (Sornette and Cauwels, 2015).

### C. Visualisation of the relative rigidity of $t_1$ vs. the sloppiness of $t_c$ using their pdf’s

The stability of  $t_1$  relative to  $t_c$  for the the four empirical bubbles described in section III.A is visualised in Fig. (5). For a given  $\bar{t}_2$  (black vertical dashed line in each panel), the blue filled function represents the *pdf* of the qualified calibrated  $\hat{t}_1^*$ ’s in a search over the grey interval up to  $\bar{t}_2 - 30$  days. The red filled function represents the corresponding pdf of qualified calibrated  $\hat{t}_c^*$ ’s. It is pleasant to observe that the pdf of  $\hat{t}_1^*$  is where one would visually locate a priori the start of the bubble, as this is the time when the price starts to present evidence of a faster-than-exponential growth. The pdf of  $\hat{t}_c^*$  is not too far from the true time of the change of regime but is often too late, except for the bubble on the Ibovespa index.

The sensitivity analysis performed around the best solution of  $\hat{t}_1^*$  and  $\hat{t}_c^*$  demonstrates that  $t_1$  is even more important than  $t_c$  for the calibration, relative to the study performed on synthetic data. Specifically, changes in  $t_1$  lead to fluctuations of the normalised sum of squared residuals spanning the interval (-2.0% to 2.0%), (0.0% to 1.0%), (-0.5% to 1.0%) and (-2.0% to 2.0%), respectively for the SSEC, SP, BM and IBovespa bubbles. In contrast, changes in  $t_c$  have negligible impact on the cost function.

Even accounting for their errors bars, one can observe that  $\lambda_3$  is at least two orders of magnitude larger than  $\lambda_4$  for all  $t_1$ ’s, corroborating the results of Sec. II.G. The parameters  $t_1$  and  $t_c$  contribute respectively to  $\lambda_3$  and  $\lambda_4$  more than 35% throughout the analysed



periods. Taken together, these features strengthen the evidence of the greater sloppiness of  $t_c$  compared to  $t_1$ , which makes the determination of the end of bubbles much more difficult than their beginning.

Finally, it is important to check how the above results generalise for different “present” times  $t_2$ , mimicking a real time situation of a developing bubble. As seen in figure 6, we consider four different values of  $t_2$  shown by the vertical dashed black lines in each panel. Note that these four choices cover most of the duration of the bubbles. For each  $t_2$ , we search the optimal  $t_1$  that minimises the cost function up to 600 days prior  $t_2$ . These intervals in which  $t_1$  is scanned are represented by the different shades of grey, one per value of  $t_2$ .

One can observe that the pdf’s of  $\hat{t}_c^*$  are quite wide and with several modes, except for the bubble on the S&P500 that burst in 2007. These modes are localised at times when the markets corrected, in addition to finding a neighbourhood of the true ends of the bubbles. In contrast, the pdf’s of  $\hat{t}_1^*$  are monomodal, very narrow and pinpoint a time when the markets start their significant ascent. For instance, for the S&P500 Index during the 1980’s, our analysis identifies two possible modes for the end of the bubble, one occurring in the last quarter of 1985 associated with a significant drawdown and the other being close to the crash on Oct. 19, 1987. Conversely, the narrow pdf of  $\hat{t}_1^*$  identifies the beginning of the bubble around mid-1984. A similar situation is observed for the SSEC Index as well as for the synthetic case.

The existence of several modes of the pdf’s of  $\hat{t}_c^*$  can be traced to the discrete scale invariance of the log-periodic oscillations (Sornette, 1998), associated with the occurrence of corrections or plateaux decorating the super-exponential growth, each of them being interpreted as a possible candidate for the end of the bubble by the calibration procedure. When used to diagnose bubbles, this confirms that the LPPLS model can determine  $t_1$  significantly more accurately than  $t_c$ .

## IV. Conclusion

We have presented systematic tests of the precision and reliability with which the beginning and end of a bubble can be determined. This has required using a specific bubble model, the log-periodic power law singularity (LPPLS) model, which represents a bubble as a transient noisy super-exponential price trajectory decorated by accelerated volatility oscillations. One of the quality of the LPPLS model is to contain the end time  $t_c$  of the bubble as a defining parameter, which can thus be estimated over various time windows. In order to estimate the beginning of a bubble, we have proposed to endogenise in the cost function the parameter  $t_1$  defining the beginning of the time window that provides the best

goodness of fit. The cost function quantifying the quality of fit of the LPPLS model has been extended to include  $t_1$ . Using the Fisher Information matrix, we have quantified the parameter uncertainty associated with the determination of both  $t_1$  and  $t_c$ . Using both synthetic data and four historical bubble cases, we find overwhelming evidence that the beginning of bubbles is much better constrained than their end. This is quantified by calculating the eigenvalues of the Hessian matrix, which characterise the shape of the cost function in the different directions in parameter space. Parameters associated with large eigenvalues are “rigid”, i.e. they tend to be well estimated. In contrast, parameters associated with small eigenvalues are “sloppy”, as large changes of their values do not impact the cost function, which is degenerate along their direction in parameter space. We find that the eigenvalues for which  $t_1$  contributes most are several orders of magnitude larger than the eigenvalues for which  $t_c$  contributes most. Practically, this implies that the beginning of financial bubbles are comparatively much easier to determine using LPPLS than their ending time  $t_c$ . Our results are robust over all four empirical bubbles and many synthetic tests, as well as when changing the time  $t_2$  (the “present”) of analysis.

Our results corroborate and extend those obtained by [Lin et al. \(2014\)](#) when studying the Black-Monday bubble of 1987. Our analysis gives support to the empirical evidence among practitioners (in particular hedge-funds ([Gurkaynak, 2008](#))), who tend to correctly diagnose on-going bubbles but in general fail to time their end.

As a side result, we have found that two structural parameters of the LPPLS model, the exponent  $m$  controlling the super-exponential growth of price and the angular log-periodic frequency  $\omega$  describing the log-periodic acceleration of volatility, are very rigid. This suggests that the LPPLS model is a reasonable candidate for describing the generating process of prices during bubbles ([Sornette, 2003](#)).

Finally, contrary to the claim in the literature that bubbles are not suppressed by arbitrageurs because they fail to agree on the beginning of the bubble ([Abreu and Brunnermeier, 2003](#)), our findings suggest that bubbles persist due to the difficulty of synchronizing on the end of bubbles.

## Acknowledgments

This work was partially supported by CNPq (Conselho Nacional de Desenvolvimento Científico e Tecnológico). The authors would like to acknowledge V. Filimonov. All calculations and figures were elaborated using open source software IPython ([Pérez and Granger, 2007](#)).

## Appendix A: calibration of the LPPLS model (3)

We use the formulation in terms of the 4 linear parameters  $A, B, C_1, C_2$  and 3 nonlinear parameter  $m, \omega, t_c$  (Filimonov and Sornette, 2013), so that the log-price given by expression (3) can be written as

$$fLPPL(\phi, t) = A + B(f) + C_1(g) + C_2(h), \quad (8)$$

where  $\phi = \{A, B, C_1, C_2, m, \omega, t_c\}$  is a  $(1 \times 7)$  vector of parameters we want to determine and

$$f \equiv (t_c - t)^m, \quad (9)$$

$$g \equiv (t_c - t)^m \cos(\omega \ln(t_c - t)), \quad (10)$$

$$h \equiv (t_c - t)^m \sin(\omega \ln(t_c - t)). \quad (11)$$

Let  $y := \vec{P} = [p_1, p_2, \dots, p_N]$  denote a price realization vector consisting of  $N$  observations and the discrete time vector  $t = [1, 2, \dots, N]$ . Fitting Eq. (8) to the logarithm of  $\vec{P}$  amounts to search for the parameter set  $\phi^*$  that yields the smallest  $N$ -dimensional distance between realisation and theory. Mathematically, using the  $L^2$  norm, we form the following sum of squares of residuals

$$F(t_c, m, \omega, A, B, C_1, C_2) = \sum_{i=1}^N \left[ \ln[P(t_i)] - A - B(f_i) - C_1(g_i) - C_2(h_i) \right]^2, \quad (12)$$

for  $i = 1, \dots, N$ . We proceed in two steps. First, slaving the linear parameters  $\{A, B, C_1, C_2\}$  to the remaining nonlinear parameters  $\phi = \{t_c, m, \omega\}$ , yields the cost function  $\chi^2(\phi)$

$$\chi^2(\phi) := F_1(t_c, m, \omega) = \min_{\{A, B, C_1, C_2\}} F(t_c, m, \omega, A, B, C_1, C_2) = F(t_c, m, \omega, \hat{A}, \hat{B}, \hat{C}_1, \hat{C}_2), \quad (13)$$

where the hat symbol  $\hat{\phantom{x}}$  indicates estimated parameters. This is obtained by solving the optimization problem

$$\{\hat{A}, \hat{B}, \hat{C}_1, \hat{C}_2\} = \arg \min_{\{A, B, C_1, C_2\}} F(t_c, m, \omega, A, B, C_1, C_2), \quad (14)$$

which can be obtained analytically by solving the following matrix equations

$$\begin{bmatrix} N & \sum f_i & \sum g_i & \sum h_i \\ \sum f_i & \sum f_i^2 & \sum f_i g_i & \sum f_i h_i \\ \sum g_i & \sum f_i g_i & \sum g_i^2 & \sum g_i h_i \\ \sum h_i & \sum f_i h_i & \sum g_i h_i & \sum h_i^2 \end{bmatrix} \begin{bmatrix} \hat{A} \\ \hat{B} \\ \hat{C}_1 \\ \hat{C}_2 \end{bmatrix} = \begin{bmatrix} \sum y_i \\ \sum y_i f_i \\ \sum y_i g_i \\ \sum y_i h_i \end{bmatrix} \quad (15)$$

Second, we solve the nonlinear optimisation problem involving the remaining nonlinear parameters  $m, \omega, t_c$ :

$$\{\hat{t}_c, \hat{m}, \hat{\omega}\} = \arg \min_{\{t_c, m, \omega\}} F_1(t_c, m, \omega). \quad (16)$$

## Appendix B: calibration of the extended set of 4 nonlinear parameters $\Phi = \{m, \omega, t_c, t_1\}$

We compute the first-order partial derivatives of Eq. (4) - i.e. the Gradient vector  $\vec{\nabla} \chi^2(\Phi)$  - with respect to each parameter as follows:

$$\begin{aligned} \frac{\partial \chi^2(\Phi)}{\partial m} &= \frac{2 \ln(t_c - t)(t_c - t)^m [\sin(\ln(t_c - t)\omega) + \cos(\ln(t_c - t)\omega) - B]}{t_2 - t_1} \\ &\times \frac{[(t_c - t)^m \sin(\ln(t_c - t)\omega) + \cos(\ln(t_c - t)\omega) - B]}{t_2 - t_1} \\ &+ \frac{C_1 + C_2 + A}{t_2 - t_1} \end{aligned} \quad (17)$$

$$\begin{aligned} \frac{\partial \chi^2(\Phi)}{\partial \omega} &= \frac{-2 \ln(t_c - t)(t_c - t)^m [\sin(\ln(t_c - t)\omega) - \cos(\ln(t_c - t)\omega)]}{t_2 - t_1} \\ &\times \frac{[(t_c - t)^m \sin(\ln(t_c - t)\omega) + \cos(\ln(t_c - t)\omega) - B]}{t_2 - t_1} \\ &+ \frac{C_1 + C_2 + A}{t_2 - t_1} \end{aligned} \quad (18)$$

$$\begin{aligned}
\frac{\partial \chi^2(\Phi)}{\partial t_c} = & \frac{-2(t_c - t)^{m-1} [(C_1\omega - C_2m) \cos(\omega \ln(t_c - t)) + Bm](t_c - t)^m}{t_2 - t_1} \\
& \times \frac{(C_2 \sin(\omega \ln(t_c - t)) + C_1 \cos(\omega \ln(t_c - t)))}{t_2 - t_1} \\
& + \frac{-B + A}{t_2 - t_1}
\end{aligned} \tag{19}$$

$$\begin{aligned}
\frac{\partial \chi^2(\Phi)}{\partial t_1} = & \frac{(-y + C_2(t_c - t)^m \sin(\ln(t_c - t)\omega) + C_1(t_c - t)^m \cos(\ln(t_c - t)\omega))}{(t_2 - t_1)^2} \\
& + \frac{B(t_c - t)^m + A}{(t_2 - t_1)^2}.
\end{aligned} \tag{20}$$

These first-order partial derivatives are collected by the Jacobian matrix  $J(\Phi)_{(N \times m)}$ ,

$$J(\Phi) = \begin{bmatrix} \frac{\partial r_i}{\partial \Phi_i} \\ \vdots \\ \frac{\partial r_i}{\partial \Phi_j} \end{bmatrix} \equiv \left[ \frac{\partial r_i}{\partial m} \frac{\partial r_i}{\partial \omega} \frac{\partial r_i}{\partial t_c} \frac{\partial r_i}{\partial t_1} \right]_{\substack{j=1,2,\dots,m; \\ i=1,2,\dots,N}}^T, \tag{21}$$

where  $r_i(\Phi) = y(t)_i - flppl(\Phi, t)_i$  are defined in Eq. (4).

Embedded within a  $m$ -dimensional Euclidean space, the Gradient vector points towards directions in which the cost increases more rapidly. At a given local minimum, the minimisation problem should not only display small  $\vec{\nabla} \chi^2(\Phi)$  values but also, the cost curvature should be convex and the residuals approximately zero. Formally, this idea is expressed as

$$\Delta \chi^2(\Phi) = \frac{1}{2} \vec{\nabla}(\Phi)^T \mathbf{H}(\Phi^*) \vec{\nabla}(\Phi) \geq 0, \tag{22}$$

where  $\mathbf{H}(\Phi^*)$  denotes the Hessian matrix expressed at the best-fit parameters. Bold letters denote either matrices or vectors. This special structure of the sum of squares of residuals allows one to approximate  $\mathbf{H}(\Phi^*)$  in terms of the fitting residuals using,

$$\frac{\partial \chi^2(\Phi)}{\partial \Phi_i \partial \Phi_j} = \sum_{i=1}^m \left( r_i \frac{\partial^2 r_i(\Phi)}{\partial \Phi_i \partial \Phi_j} + \frac{\partial r_i(\Phi)}{\partial \Phi_i} \frac{\partial r_i(\Phi)}{\partial \Phi_j} \right). \tag{23}$$

Since Eq. (22) holds, we therefore skip the calculation of second-order derivatives and compute  $\mathbf{H}(\Phi^*)$  solely using the Jacobian (Machta et al., 2013; Tsay, 2010),

$$\mathbf{H}|_* \equiv \mathbf{J}^T \mathbf{J} = \sum_{i=1}^N (\vec{\nabla} r_i(\Phi^*)) (\vec{\nabla} r_i(\Phi^*))^T. \tag{24}$$

At the best-fit, the Hessian is always *symmetric*, positive-definite and has entries according to

$$H_{i,j}^{\chi^2(\Phi^*)} = \begin{bmatrix} \frac{\partial^2 r_i(\Phi)}{\partial m, \partial m} & \frac{\partial^2 r_i(\Phi)}{\partial m, \partial \omega} & \frac{\partial^2 r_i(\Phi)}{\partial m, \partial t_c} & \frac{\partial^2 r_i(\Phi)}{\partial m, \partial t_1} \\ \frac{\partial^2 r_i(\Phi)}{\partial \omega, \partial m} & \frac{\partial^2 r_i(\Phi)}{\partial \omega, \partial \omega} & \frac{\partial^2 r_i(\Phi)}{\partial \omega, \partial t_c} & \frac{\partial^2 r_i(\Phi)}{\partial \omega, \partial t_1} \\ \frac{\partial^2 r_i(\Phi)}{\partial t_c, \partial m} & \frac{\partial^2 r_i(\Phi)}{\partial t_c, \partial \omega} & \frac{\partial^2 r_i(\Phi)}{\partial t_c, \partial t_c} & \frac{\partial^2 r_i(\Phi)}{\partial t_c, \partial t_1} \\ \frac{\partial^2 r_i(\Phi)}{\partial t_1, \partial m} & \frac{\partial^2 r_i(\Phi)}{\partial t_1, \partial \omega} & \frac{\partial^2 r_i(\Phi)}{\partial t_1, \partial t_c} & \frac{\partial^2 r_i(\Phi)}{\partial t_1, \partial t_1} \end{bmatrix}. \quad (25)$$

Derivatives are calculated using a *centered finite-difference scheme*,

$$\chi^2(\Phi^*)' \approx \frac{\chi^2(\Phi^* + h) - \chi^2(\Phi^* - h)}{2h}, \quad (26)$$

with step-size  $h$  varying according to information provided by the Gradient. The choice of  $h$  should neither be too small or too large.

# REFERENCES

- Abreu, D., and K. Brunnermeier, 2003, Bubbles and crashes, *Econometrica* 1, 173–204.
- Bak, Per, Chao Tang, and Kurt Wiesenfeld, 1988, Self-organized criticality, *Phys. Rev. A* 3, 364–374.
- Barberis, Nicholas, Andrei Shleifer, and Robert Vishny, 1998, A model of investor sentiment, *Journal of Financial Economics* 49, 307–343.
- Blanchard, Olivier J., and Mark W. Watson, 1982, Bubbles, rational expectations and financial markets, Working Paper 945, National Bureau of Economic Research.
- Bree, D., D. Challet, and P. Peirano, 2013, Prediction accuracy and sloppiness of log-periodic functions, *Quantitative Finance* 3, 275–280.
- Brown, Kevin S., and James P. Sethna, 2003, Statistical mechanical approaches to models with many poorly known parameters, *Phys. Rev. E* 68, 021904.
- Brunnermeier, Markus K., and Stefan Nagel, 2004, Hedge funds and the technology bubble, *Journal of Finance* 59, 2013–2040.
- Brunnermeier, Markus K., and Martin Oehmke, 2013, Bubbles, financial crises, and systemic risk, *Handbook of the Economics of Finance* 2 (Part B), 1221–1288.
- Filimonov, V., and D. Sornette, 2013, A stable and robust calibration scheme of the log-periodic power law model, *Physica A* 17, 3698–3707.
- Geraskin, Petr, and Dean Fantazzini, 2011, Everything you always wanted to know about log-periodic power laws for bubble modeling but were afraid to ask, *The European Journal of Finance* 19, 366–391.
- Graf v. Bothmer, H.-C., and C. Meister, 2003, Predicting critical crashes? a new restriction for the free variables, *Physica A* 320, 539–547.



- Gurkaynak, R., 2008, Econometric tests of asset price bubbles: taking stock, *Journal of Economic Surveys* 22, 166–186.
- Harrison, Michael, and D. M. Kreps, 1978, Speculative investor behavior in a stock-market with heterogeneous expectations, *Quarterly Journal of Economics* 92, 323–336.
- Huang, Y., A. Johansen, M. W. Lee, H. Saleur, and D. Sornette, 2000, Artifactual log-periodicity in finite-size data: Relevance for earthquake aftershocks, *J. Geophys. Res.* 105, 25451–25471.
- Hüsler, A., D. Sornette, and C. H. Hommes, 2012, Super-exponential bubbles in lab experiments: evidence for anchoring over-optimistic expectations on price, *Journal Economic Behavior & Organization* 92, 304–316.
- Jiang, Zhi-Qiang, Wei-Xing Zhou, Didier Sornette, Ryan Woodard, Ken Bastiaensen, and Peter Cauwels, 2010, Bubble diagnosis and prediction of the 2005-2007 and 2008-2009 chinese stock market bubbles, *Journal of Economic Behavior and Organization* 74, 149–162.
- Johansen, A., O. Ledoit, and D. Sornette, 2000, Crashes as critical points, *International Journal of Theoretical and Applied Finance* 2, 219–255.
- Johansen, A., and D. Sornette, 2010, Shocks, crashes and bubbles in financial markets, *Brussels Economic Review (Cahiers économiques de Bruxelles)* 53, 201–253.
- Kaizoji, Taisei, and Didier Sornette, 2010, Market bubbles and crashes, *Encyclopedia of Quantitative Finance* (Wiley), (long version at <http://arXiv.org/abs/0812.2449>).
- Kindleberger, C. P., 1978, *Manias, Panics and Crashes: A History of Financial Crises*, third edition (Macmillan, London).
- Lin, L., R. E. Ren, and D. Sornette, 2014, The volatility-confined lppl model: A consistent

- model of ‘explosive’ financial bubbles with mean-reverting residuals, *International Review of Financial Analysis* 33, 210–222.
- Machta, B., R. Chachra, M. Transtrum, and J. Sethna, 2013, Parameter space compression underlies emergent theories and predictive models, *Science* 342, 604–607.
- Marquardt, D.W., 1962, An algorithm for least-squares estimation of nonlinear parameters, *SIAM Journal on Applied Mathematics* 2, 431–441.
- Minsky, and Hyman, 1974, The modeling of financial instability: An introduction, *Proceedings of the fifth annual Pittsburgh conference* .
- Pérez, Fernando, and Brian E. Granger, 2007, IPython: a system for interactive scientific computing, *Comput Sci Eng* 9, 21–29.
- Saleur, H., and D. Sornette, 1996, Complex exponents and log-periodic corrections in frustrated systems, *J.Phys.I France* 6, 327–355.
- Samuelson, Paul, 1965, Proof that properly anticipated prices fluctuate randomly, *Industrial management review* 6, 41–49.
- Shiller, R., 2000, *Irrational exuberance* (Princeton University Press, Princeton, NJ).
- Shiller, R. J., 1981, Do stock prices move too much to be justified by subsequent changes in dividends?, *American Economic Review* 71, 421–436.
- Shleifer, Andrei, 2000, *Inefficient markets, an introduction to behavioral finance* (Clarendon Lectures in Economics, Oxford University Press).
- Sornette, D., 1998, Discrete scale invariance and complex dimensions, *Physics Reports* 297, 239–270, (extended version at <http://xxx.lanl.gov/abs/cond-mat/9707012>).
- Sornette, D., 2014, Physics and financial economics (1776-2014): Puzzles, ising and agent-based models, *Report of Progress in Physics* 77, 062001.

- Sornette, D., and P. Cauwels, 2014, 1980-2008: The illusion of the perpetual money machine and what it bodes for the future, *Risks* 2, 103–131.
- Sornette, D., and P. Cauwels, 2015, Financial bubbles: mechanisms, diagnostics and state of the world, *Review of Behavioral Economics* 2, 279–305.
- Sornette, D., and A. Johansen, 2001, Significance of log-periodic precursors to financial crashes, *Quantitative Finance* 1, 452–471.
- Sornette, D., A. Johansen, and J. P. Bouchaud, 1995, Stock market crashes, precursors and replicas, *Journal of Physics* 6, 167–175.
- Sornette, Didier, 2003, *Why stock markets crash: Critical events in complex financial systems* (Princeton University Press, New Jersey).
- Sornette, Didier, and Ryan Woodard, 2010, Financial bubbles, real estate bubbles, derivative bubbles, and the financial and economic crisis (2009), *Proceedings of APFA7 (Applications of Physics in Financial Analysis)*, “Econophysics Approaches to Large-Scale Business Data and Financial Crisis” Misako Takayasu, Tsutomu Watanabe and Hideki Takayasu, eds., Springer, 101–148.
- Transtrum, M., and J. Sethna, 2012, Improvements to the levenberg-marquardt algorithm for nonlinear least-squares minimization, *arXiv preprint* <http://arxiv.org/abs/1201.5885>.
- Transtrum, Mark K., Benjamin B. Machta, and James P. Sethna, 2011, Geometry of nonlinear least squares with applications to sloppy models and optimization, *Phys. Rev. E* 83, 673–701.
- Tsay, R., 2010, *Analysis of financial time-series*, Wiley series in probability and statistics, third edition (Wiley).
- Xiong, W., 2013, Bubbles, crisis and heterogeneous beliefs, *Handbook on Systemic Risk*

(*Cambridge University Press*), edited *Jean-Pierre Fouque and Joseph A. Langsam*, Chapter 24, 663–713.

<i>lppls synthetic</i>									
Hessian, $\mathbf{H}(\Phi^*)$					$\lambda$	Eigenvectors, $\vec{v}$			
	$m$	$\omega$	$t_c$	$t_1$		$m$	$\omega$	$t_c$	$t_1$
$m$	0.3860				$3.86 \bullet 10^{-1}$	<b>0.999</b>	0.021	0.002	$1.23e^{-4}$
$\omega$	0.0082	$7.81e^{-4}$			$6.05 \bullet 10^{-4}$	0.021	<b>0.999</b>	0.008	0.002
$t_c$	$2.98e^{-5}$	$6.11e^{-7}$	$6.60e^{-9}$		$7.00 \bullet 10^{-6}$	$7.72e^{-5}$	-0.002	0.001	<b>1.000</b>
$t_1$	0.0010	$2.61e^{-5}$	$6.02e^{-8}$	$9.63e^{-6}$	$1.71 \bullet 10^{-9}$	0.0026	0.008	<b>1.000</b>	0.001
Hessian, $\mathbf{H}(\phi^*)$					$\lambda$	Eigenvectors, $\vec{v}$			
	$m$	$\omega$	$t_c$			$m$	$\omega$	$t_c$	
$m$	0.3102				$3.10 \bullet 10^{-1}$	<b>0.999</b>	0.017		$1.18e^{-4}$
$\omega$	0.0054	$5.77e^{-4}$			$4.84 \bullet 10^{-4}$	0.017	<b>0.999</b>		0.002
$t_c$	$2.55e^{-5}$	$5.71e^{-7}$	$5.75e^{-9}$		$1.54 \bullet 10^{-9}$	$8.20e^{-5}$	0.002		<b>1.000</b>

**Table I** Hessian matrix (left columns), eigenvalues  $\lambda$  (middle column) and corresponding eigenvectors  $\vec{v}$  (right columns), for the best LPPLS fits of the synthetic price time series generated as explained in section II.G using  $\chi^2(\phi)$  and  $\chi^2(\Phi)$  in the full window shown in Fig. 1(a) corresponding to  $[t_1 = \text{Jan. 1981 to } t_2 = \text{Aug. 1987}]$  (represented as  $[\text{Date} = 1 : \text{Date} = 1100]$ ). The top rows correspond to the extended cost function (4) endogenizing  $t_1$  as a parameter to be determined. The bottom rows correspond to the case of a fixed  $t_1$  with cost function (12).

SSEC											
					$t_1^* \approx Feb. 2005, t^2 \approx Oct. 2007$						
Hessian, $H(\Phi^*)$					$\lambda$		Eigenvectors, $\vec{v}$				
	$m$	$\omega$	$t_c$	$t_1$			$m$	$\omega$	$t_c$	$t_1$	
$m$	$4.98e^0$				$4.98 \bullet 10^0$		<b>0.999</b>	0.024	0.004	0.001	
$\omega$	$1.19e^{-1}$	$3.41e^{-2}$			$3.14 \bullet 10^{-2}$		0.024	<b>0.999</b>	0.008	0.014	
$t_c$	$3.24e^{-2}$	$6.23e^{-2}$	$7.33e^{-4}$		$3.48 \bullet 10^{-4}$		0.000	0.014	0.007	<b>0.999</b>	
$t_1$	$2.33e^{-3}$	$5.00e^{-3}$	$4.51e^{-6}$	$7.90e^{-3}$	$2.74 \bullet 10^{-6}$		0.004	0.008	<b>0.999</b>	0.007	
S&P 500(SP)											
					$t_1^* \approx Dec. 2003, t^2 \approx Jul. 2007$						
Hessian, $H(\Phi^*)$					$\lambda$		Eigenvectors, $\vec{v}$				
	$m$	$\omega$	$t_c$	$t_1$			$m$	$\omega$	$t_c$	$t_1$	
$m$	$1.68e^1$				$1.68 \bullet 10^1$		<b>1.000</b>	0.006	0.004	0.001	
$\omega$	$1.08e^{-1}$	$5.00e^{-3}$			$5.11 \bullet 10^{-3}$		0.006	<b>0.999</b>	0.038	0.002	
$t_c$	$6.00e^{-3}$	$8.33e^{-2}$	$3.71e^{-3}$		$1.36 \bullet 10^{-4}$		0.000	0.002	0.0012	<b>1.000</b>	
$t_1$	$1.61e^{-2}$	$2.98e^{-4}$	$8.4e^{-8}$	$6.00e^{-6}$	$6.42 \bullet 10^{-8}$		0.000	0.038	<b>0.999</b>	0.001	
S&P 500(BM)											
					$t_1^* \approx Mar. 1984, t^2 \approx Aug. 1987$						
Hessian, $H(\Phi^*)$					$\lambda$		Eigenvectors, $\vec{v}$				
	$m$	$\omega$	$t_c$	$t_1$			$m$	$\omega$	$t_c$	$t_1$	
$m$	$3.57e^1$				$3.50 \bullet 10^1$		<b>0.999</b>	0.011	0.002	0.000	
$\omega$	$3.88e^0$	$6.39 e^{-1}$			$5.96 \bullet 10^{-1}$		0.011	<b>0.998</b>	0.013	0.002	
$t_c$	$2.61e^{-2}$	$8.44e^{-2}$	$9.12e^{-2}$		$5.69 \bullet 10^{-3}$		0.001	0.002	0.0012	<b>1.000</b>	
$t_1$	$7.10e^{-1}$	$6.80e^{-3}$	$3.78e^{-7}$	$1.32e^{-4}$	$8.94 \bullet 10^{-7}$		0.002	0.013	<b>0.999</b>	0.001	
IBovespa											
					$t_1^* \approx Jun. 2003, t^2 \approx Jan. 2004$						
Hessian, $H(\Phi^*)$					$\lambda$		Eigenvectors, $\vec{v}$				
	$m$	$\omega$	$t_c$	$t_1$			$m$	$\omega$	$t_c$	$t_1$	
$m$	$2.26e^0$				$2.26 \bullet 10^0$		<b>0.999</b>	0.014	0.003	0.001	
$\omega$	$3.11e^{-1}$	$1.08e^{-2}$			$1.03 \bullet 10^{-2}$		0.014	<b>0.992</b>	0.0341	0.014	
$t_c$	$7.33e^{-3}$	$9.02e^{-2}$	$5.02e^{-3}$		$1.70 \bullet 10^{-4}$		0.001	0.015	0.030	<b>0.999</b>	
$t_1$	$7.33e^{-3}$	$8.54e^{-4}$	$9.43e^{-7}$	$1.70e^{-4}$	$9.82 \bullet 10^{-7}$		0.003	0.033	<b>0.989</b>	0.031	

**Table II** Hessian matrix, eigenvalues and corresponding eigenvectors for the best LPPLS fits using Eq (4) of the financial bubbles described in section III.A in the time windows  $[t_1^* : t_2]$  given in the table for each bubble. The numbers in boldface indicate the parameters that contribute the most to their eigenvectors.

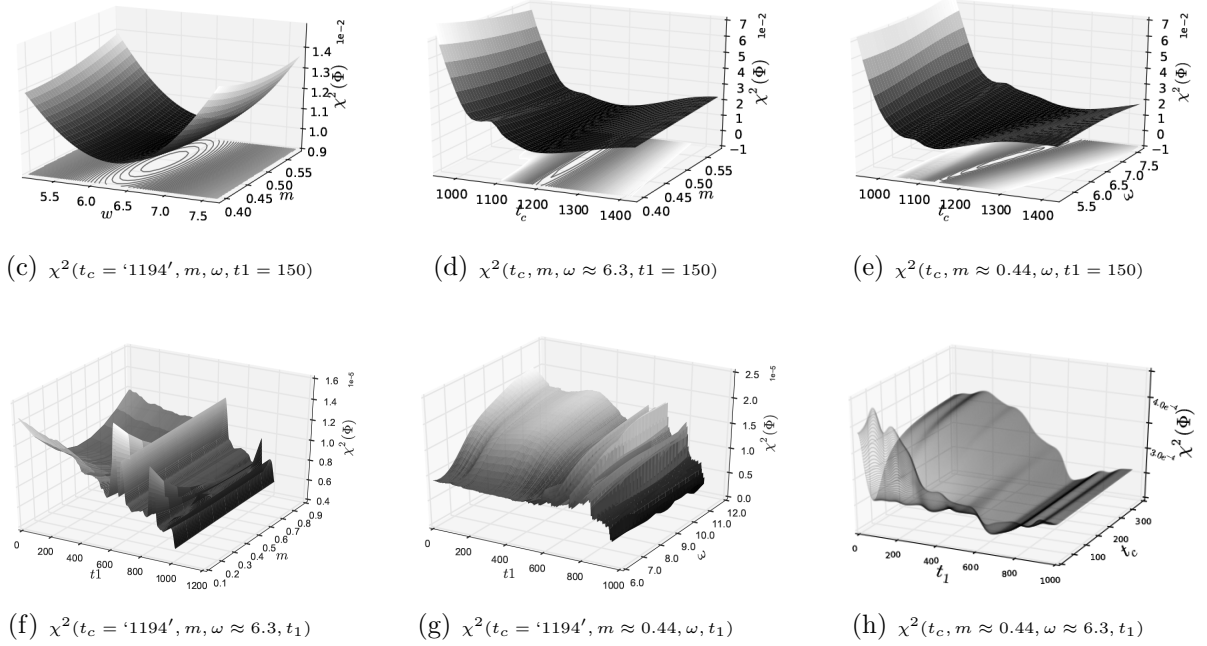
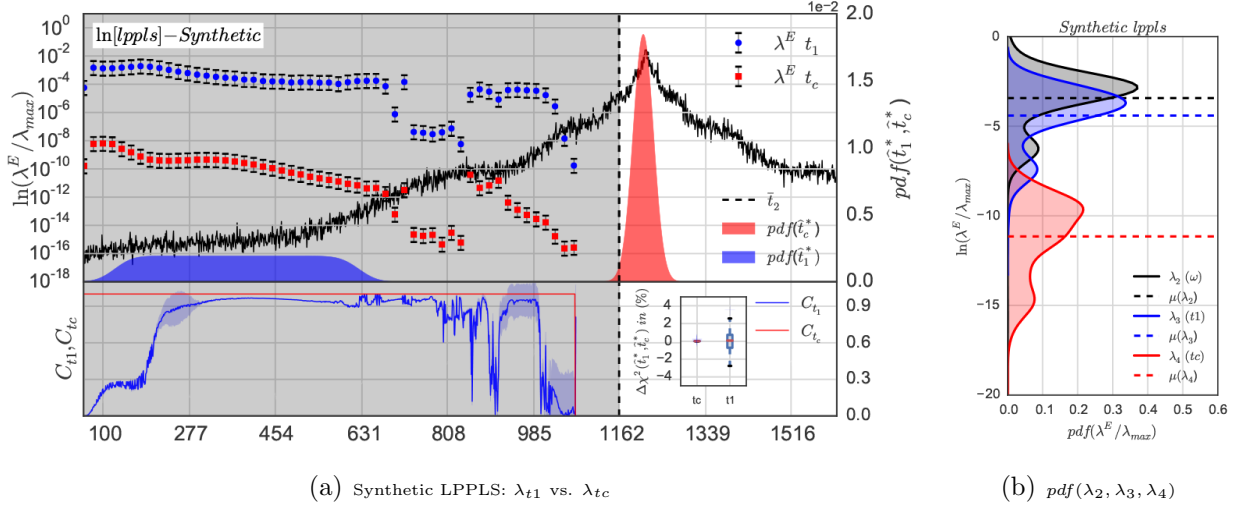


**Figure 1.** Quantification of the relative sloppiness of  $t_c$  and  $t_1$  in synthetic data: (panel 1(a)): a synthetic noisy LPPLS price time series generated as described in the main text is shown with the black continuous line. Here, the  $x$ -axis denote values of the beginning  $t_1$  of the window in which the calibration is performed at a fixed  $\bar{t}_2$ . The blue circles and red squares show the normalised eigenvalues ( $\lambda$ ) of the Hessian matrix  $H(\Phi^*)$  estimated at the best-fit, which correspond mainly to the directions  $t_1$  and  $t_c$  in parameter space, (See Fig (5) for precise quantification). Errors bars for each parameter represent  $\lambda_i^E \pm \sigma(\lambda_i^E)$  over 100 realisations (corresponding to 100 generations of the noise). The relative contribution (see Eq. 7) of  $t_1$  and  $t_c$  at eigenvalues  $\lambda_3$  and  $\lambda_4$  is depicted using coloured lines within the grey-shaded area. Coloured  $pdf$ 's denote qualified values of  $t_1$  and  $t_c$  at  $\bar{t}_2$ . The inset box-plot shows the normalised cost change in % terms when  $t_1$  (respectively  $t_c$ ) are perturbed over the ensemble of  $\hat{t}_1^*$  (respectively  $\hat{t}_c^*$ ). Panel 1(b) shows the distributions over the ensemble of  $t_1$  values of the Hessian eigenvalues for the aggregated LPPLS fits performed in the synthetic data. From top to bottom, the  $y$ -axis display the hierarchy (rigid to sloppy) of parameters that govern the model output. Panels 1(c)-1(h): cross-sections of the cost function  $\chi^2(\Phi)$  at the best-fit window ( $w \equiv ||t_1^* : t_2^*||$ , i.e. for the window starting at the fitted  $t_1$  for the fixed  $t_2 = 150$ ) in the planes  $(m, \omega)$ ,  $(t_c, \omega)$ ,  $(t_c, m)$ ,  $(t_1, m)$ ,  $(t_c, \omega)$  and  $(t_1, t_c)$  respectively.



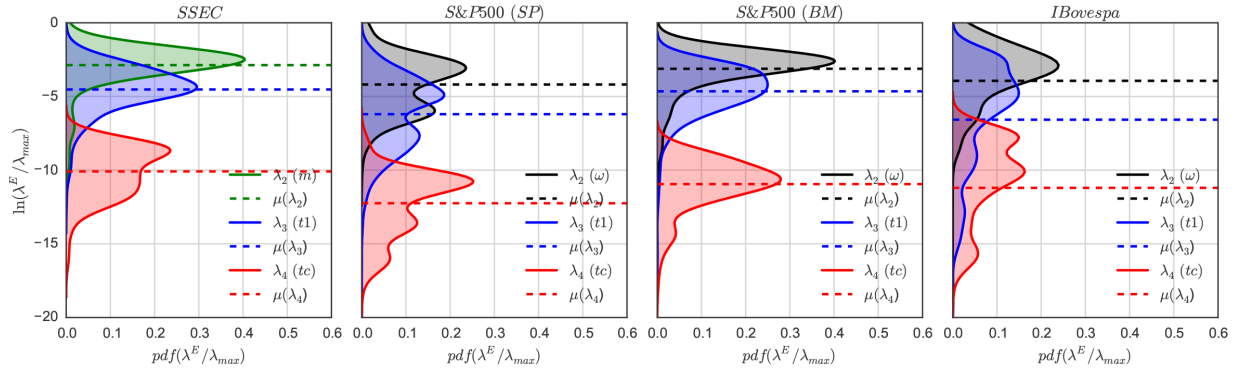


**Figure 2.** Probability density functions (pdf) of the normalized eigenvalues  $\lambda_2/\lambda_1$ ,  $\lambda_3/\lambda_1$  and  $\lambda_4/\lambda_1$  over the ensemble of windows obtained by scanning  $t_1$  for the four empirical bubbles described in section III.A. The horizontal dashed lines indicate the mean values of the distributions. The colors of the *pdf*'s encode the parameter that dominates its corresponding eigenvalue: green for  $m$ , grey for  $\omega$ , blue for  $t_1$  and red for  $t_c$ .

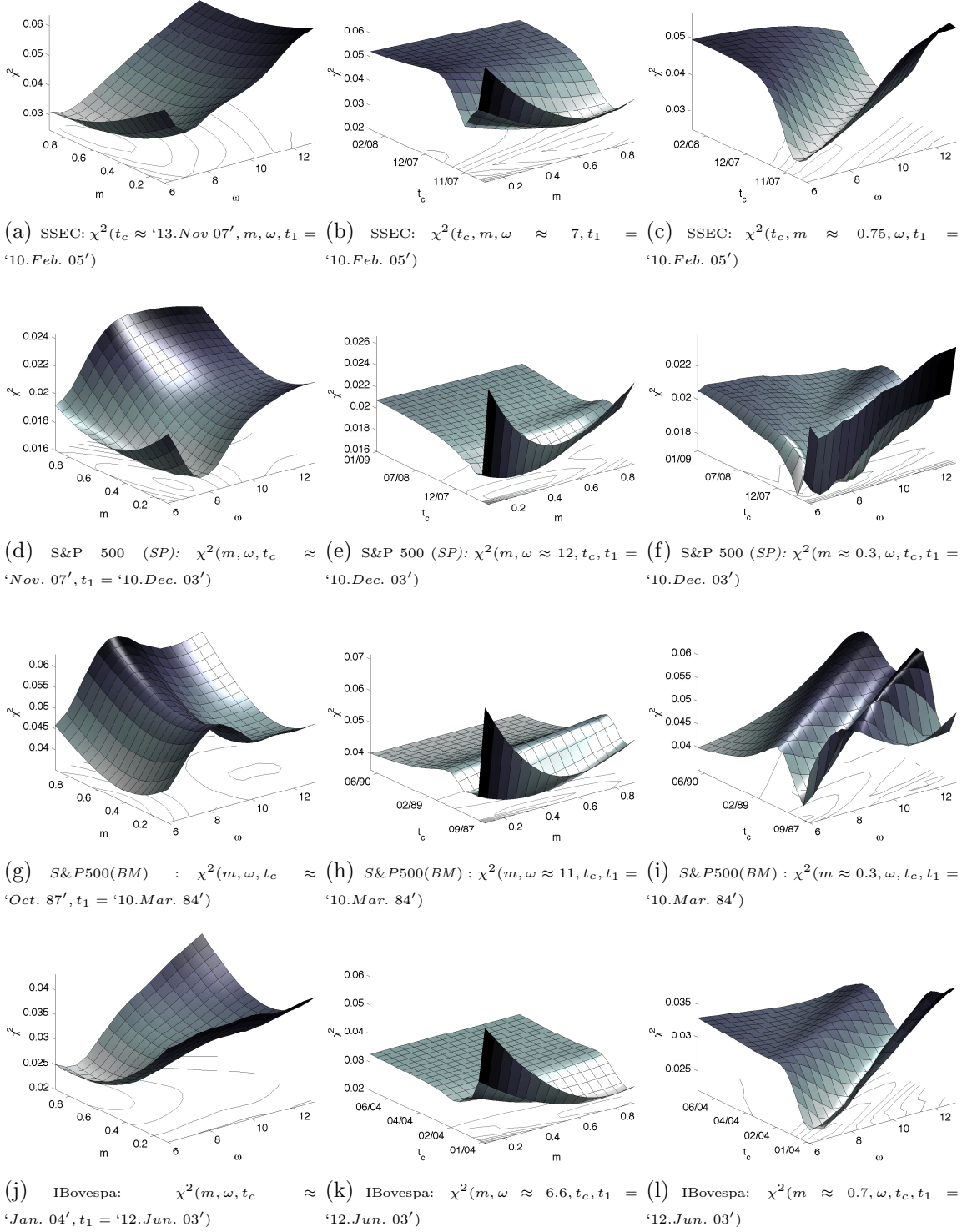
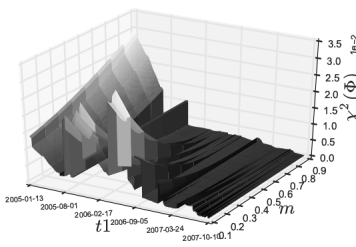
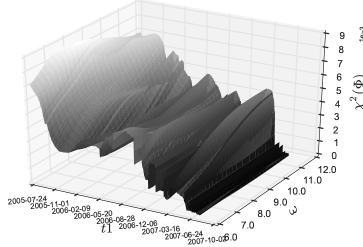


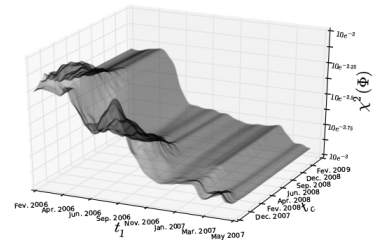
**Figure 3.** Cross-sections of the cost function  $\chi^2(\Phi)$  for the four studied empirical bubbles described in section III.A along the three different pairs of structural parameters  $(m, \omega)$ ,  $(t_c, m)$  and  $(t_c, \omega)$ . Small (resp. large) values for the cost function correspond to lighter (resp. darker) colours and depict parameter domains giving better fits.



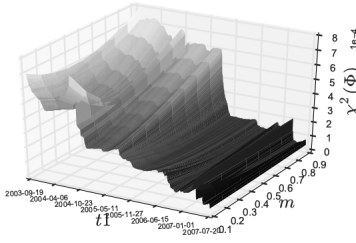
(a) SSEC:  $\chi^2(t_c \approx '13.Nov. 07', m, \omega, t_1)$



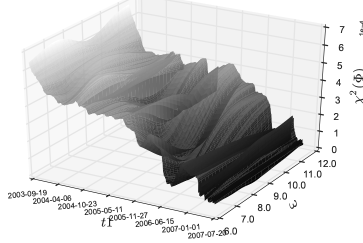
(b) SSEC:  $\chi^2(t_c, m, \omega \approx 7, t_1)$



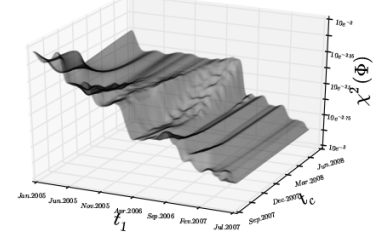
(c) SSEC:  $\chi^2(t_c, m \approx 0.75, \omega, t_1)$



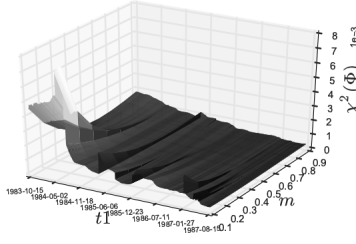
(d) S&P 500 (SP):  $\chi^2(m, \omega, t_c \approx 'Nov. 07', t_1)$



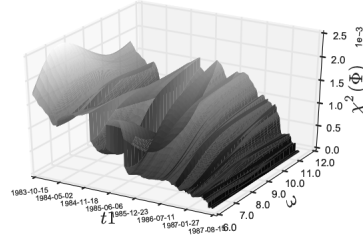
(e) S&P 500 (SP):  $\chi^2(m, \omega \approx 12, t_c, t_1)$



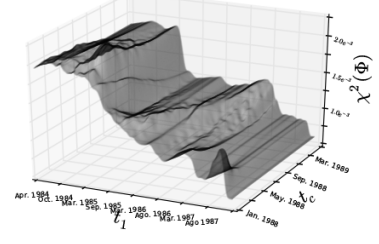
(f) S&P 500 (SP):  $\chi^2(m \approx 0.3, \omega, t_c, t_1)$



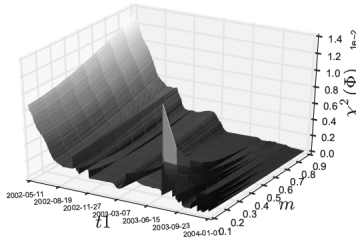
(g) S&P500(BM) :  $\chi^2(m, \omega, t_c \approx 'Oct. 87', t_1)$



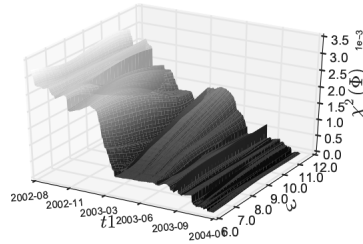
(h) S&P500(BM) :  $\chi^2(m, \omega \approx 11, t_c, t_1)$



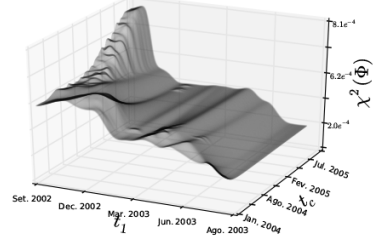
(i) S&P500(BM) :  $\chi^2(m \approx 0.3, \omega, t_c, t_1)$



(j) IBovespa:  $\chi^2(m, \omega, t_c \approx 'Jan. 04', t_1)$



(k) IBovespa:  $\chi^2(m, \omega \approx 6.6, t_c, t_1)$



(l) IBovespa:  $\chi^2(m \approx 0.7, \omega, t_c, t_1)$

**Figure 4.** Cross-sections of the cost function  $\chi^2(\Phi)$  for the four studied empirical bubbles described in section III.A along the three different pairs of parameters  $(t_1, m)$ ,  $(t_1, \omega)$  and  $(t_1, t_c)$ , outlining the dependence on the parameter  $t_1$  representing the beginning of the bubble. Small (resp. large) values for the cost function correspond to lighter (resp. darker) colours and depict parameter domains giving better fits.

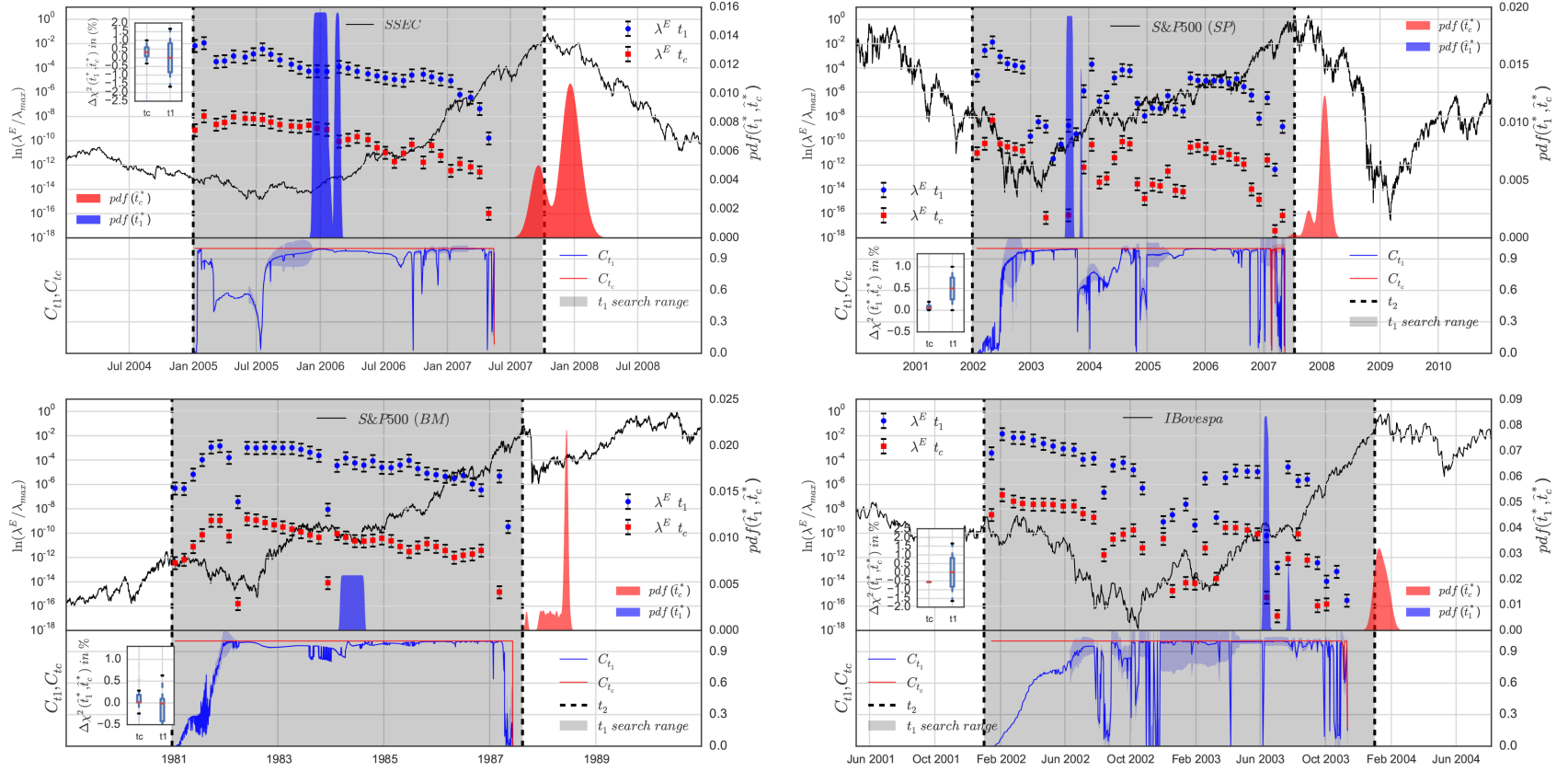


**Figure 5.** : Quantification of the relative sloppiness of  $t_c$  and  $t_1$  for the four empirical bubbles described in section III.A. The logarithm of their price as a function of time is shown by the black continuous line in each panel. The blue circles and red squares show the normalised eigenvalues  $\lambda_3^E$  and  $\lambda_4^E$  of the Hessian matrix  $H(\Phi^*)$  estimated for the best-fit, respectively mainly associated with  $t_1$  and  $t_c$ , as a function of  $t_1$  for a fixed  $t_2$  indicated by the black vertical dashed line (See Fig (11 in the Supplementary Materials) for a precise quantification of the weight of each parameter for each eigenvalue). The errors bars represent  $\pm$  one-sigma interval around the mean values, obtained over 100 estimations. The relative contribution defined by expression (7) of  $t_1$  to the eigenvalue  $\lambda_3$  and of  $t_c$  to  $\lambda_4$  are shown using vertical coloured lines inside the grey-shaded area. The box-plots in the inset show the normalised cost change in percent when  $t_1$  (respectively  $t_c$ ) are sampled over the ensemble of calibrated  $\hat{t}_1^*$  (respectively  $\hat{t}_c^*$ ).

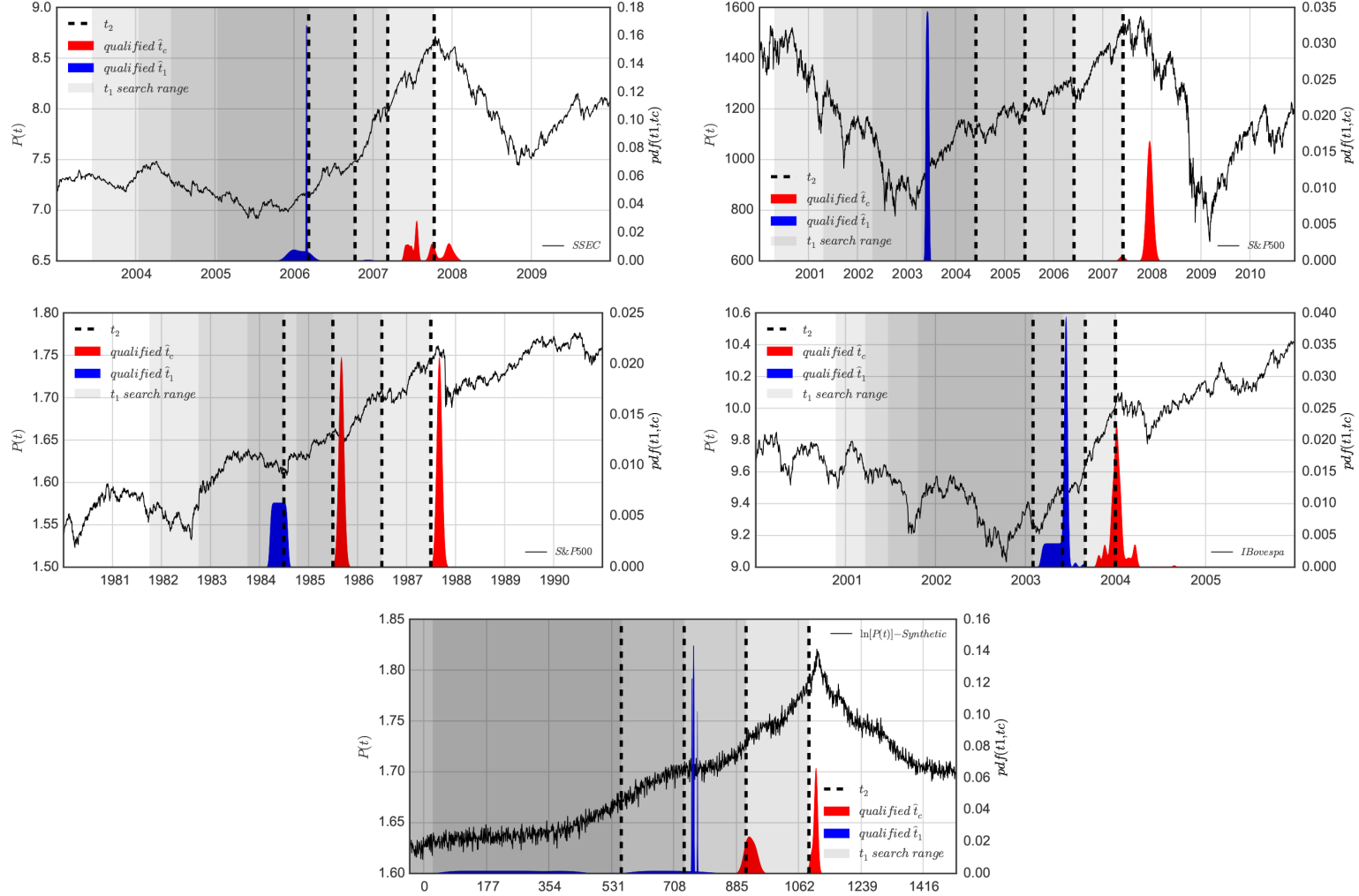
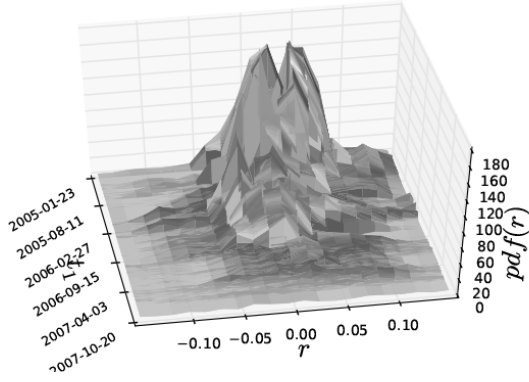


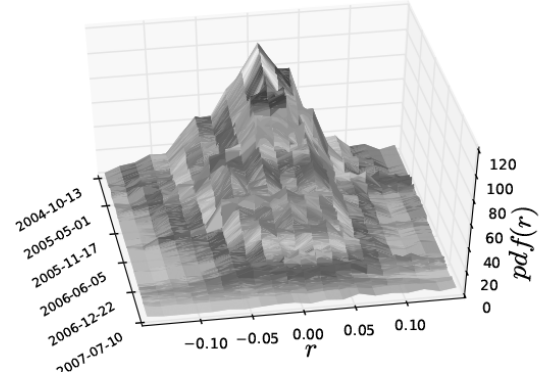
**Figure 6.** Analysis of the four bubbles described in section III.A as well as for a synthetic bubble, for four different values of  $t_2$  shown by the vertical dashed black lines in each panel. The red (resp. blue) filled curve represents the pdf of  $\hat{t}_c^*$  (resp.  $\hat{t}_1^*$ ) over the set of time windows obtained from the four  $t_2$ 's by scanning  $t_1$  over their corresponding grey shaded area, each of the same width of 600 days. The pdf's are represented using a kernel method with bandwidth  $\approx 0.1$  year.



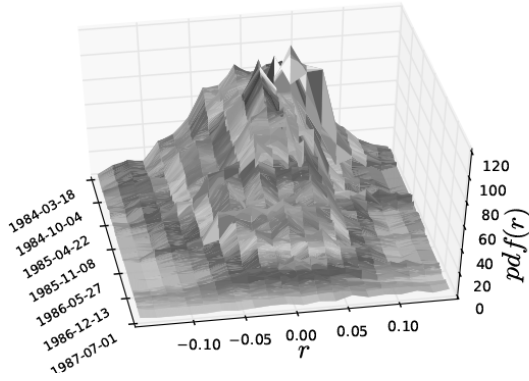
## Supplementary Materials



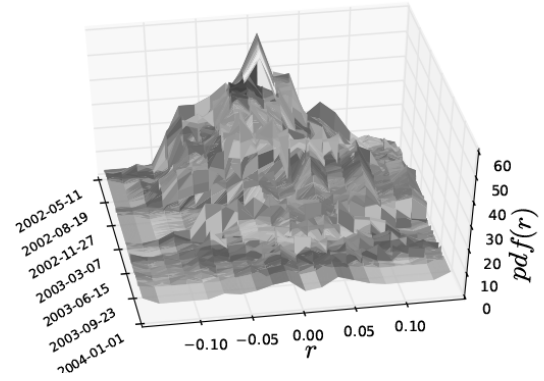
(a) SSEC



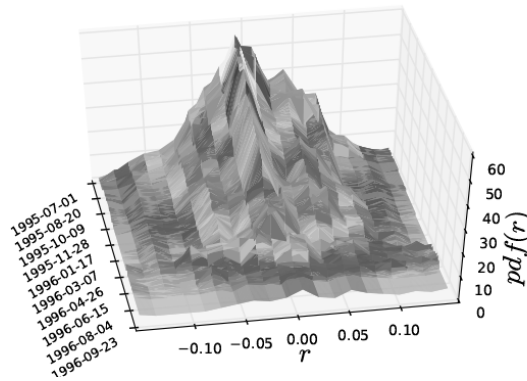
(b)  $S\&P500(SP)$



(c)  $S\&P500(BM)$



(d) IBovespa



(e) Synthetic Fitting residuals,  $r$

**Figure 7.** Probability density functions ( $pdf$ ) of the residuals  $r(t)$ 's defined in (4) for various values of  $t_1$  (y-axis) for the four studied empirical bubbles described in section III.A and one synthetic data discussed in the text.



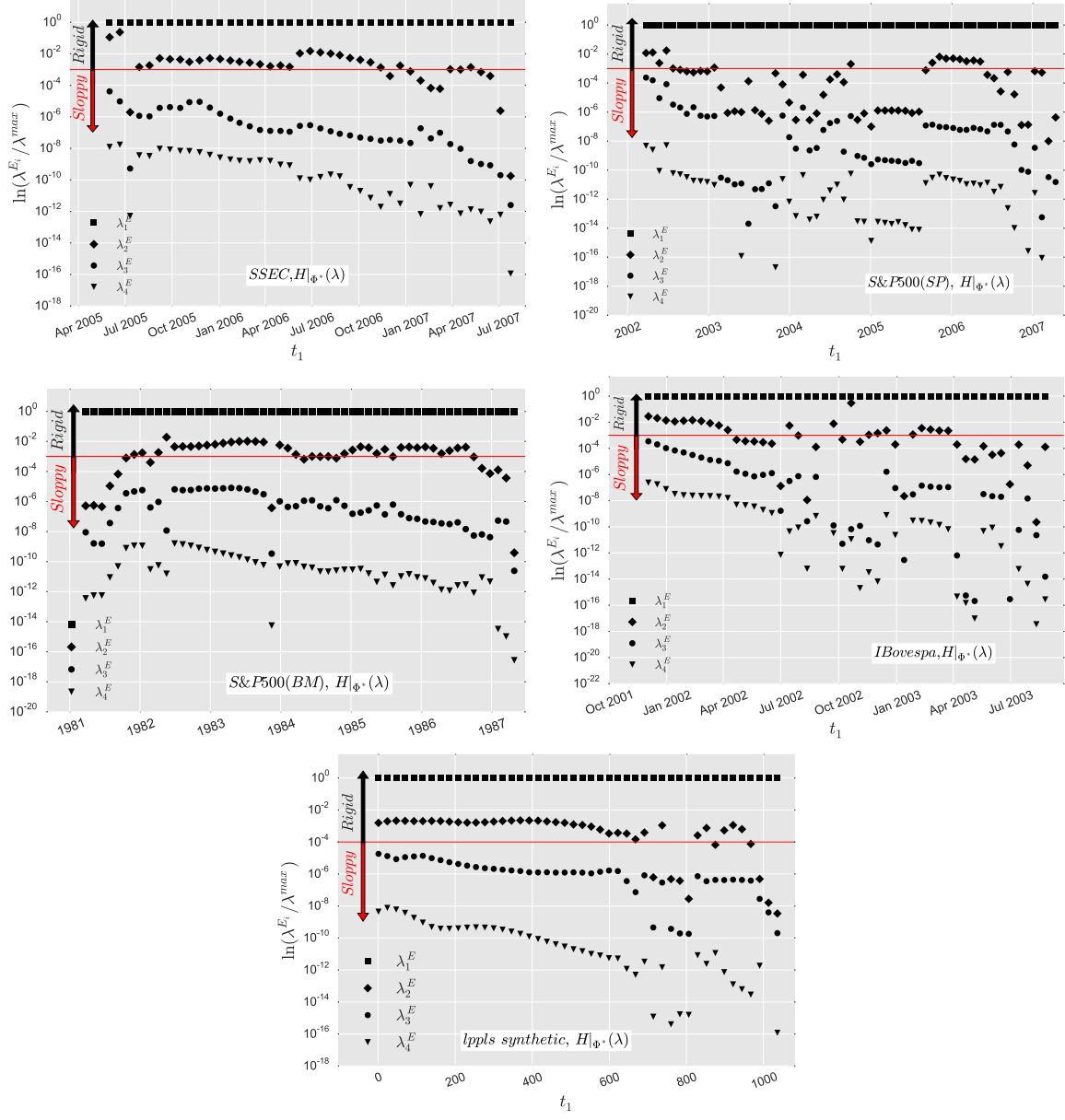


**Figure 8.** Eigenvalues ( $\lambda$ ) of  $H|_{\Phi^*}$  as a function of  $t_1$  for the four studied empirical bubbles described in section III.A and one synthetic data discussed in the text, when using the extended cost function (4). The contribution of each parameter in each  $\lambda$  is given in fig. (11.)

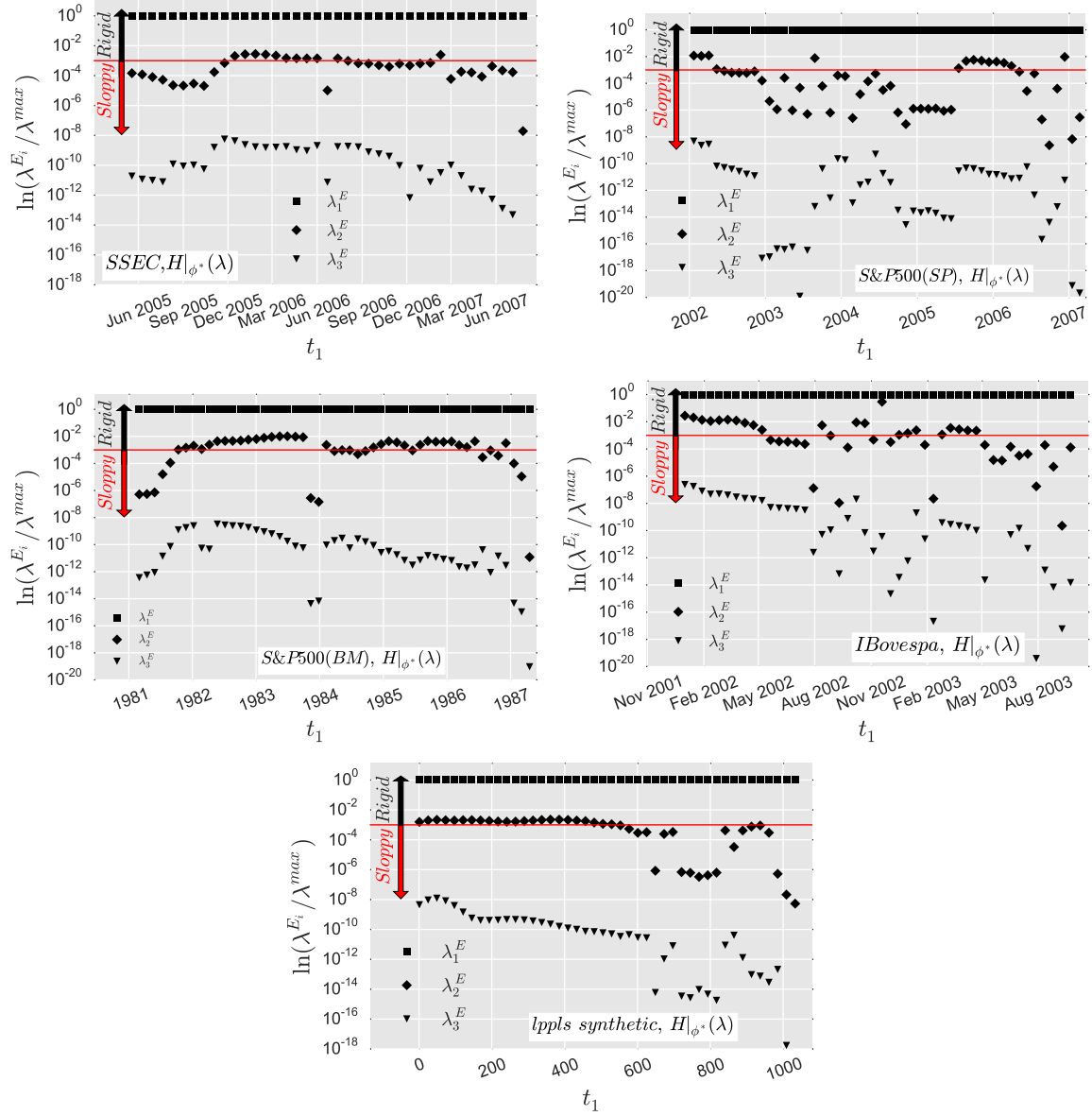


**Figure 9.** Eigenvalues ( $\lambda$ ) of  $H|_{\phi^*}$  as a function of  $t_1$  for the four studied empirical bubbles described in section III.A and one synthetic data discussed in the text, using the original cost function (12). The contribution of each parameter along each  $\lambda$  is given by fig. (10). The dynamical structure of eigenvalues is very similar to what is observed in Fig 8 when using the extended cost function.

<i>SSEC</i>								
$t_1^* \approx \text{Feb. 2005}, t^2 \approx \text{Oct. 2007}$								
Hessian $\mathbf{H}(\phi^*)$			$\lambda$			Eigenvectors $\vec{v}$		
	$m$	$\omega$	$t_c$			$m$	$\omega$	$t_c$
$m$	1.7504			$3.04 \bullet 10^0$		<b>-0.9991</b>	0.0418	-0.0015
$\omega$	-0.3439	0.0990		$3.16 \bullet 10^{-2}$		0.0418	<b>0.9990</b>	-0.0140
$t_c$	0.0065	-0.0042	0.0002	$2.76 \bullet 10^{-6}$		$-8.82 e^{-4}$	0.0140	<b>0.9999</b>
<i>S&amp;P500 (SP)</i>								
$t_1^* \approx \text{Dec. 2003}, t^2 \approx \text{Jul. 2007}$								
Hessian $\mathbf{H}(\phi^*)$			$\lambda$			Eigenvectors $\vec{v}$		
	$m$	$\omega$	$t_c$			$m$	$\omega$	$t_c$
$m$	17.713			$1.77 \bullet 10^1$		<b>-1.0000</b>	-0.0064	$-5.42 e^{-5}$
$\omega$	0.1133	0.0063		$5.61 \bullet 10^{-3}$		-0.0064	<b>1.0000</b>	-0.0030
$t_c$	0.0013	$2.51 e^{-5}$	$2.18 e^{-7}$	$7.19 \bullet 10^{-8}$		$-7.35 \bullet 10^{-5}$	0.0030	<b>1.0000</b>
<i>S&amp;P500 (BM)</i>								
$t_1^* \approx \text{Mar. 1984}, t^2 \approx \text{Aug. 1987}$								
Hessian $\mathbf{H}(\phi^*)$			$\lambda$			Eigenvectors $\vec{v}$		
	$m$	$\omega$	$t_c$			$m$	$\omega$	$t_c$
$m$	353.39			$3.53 \bullet 10^2$		<b>-0.9999</b>	0.0117	$-9.95 e^{-5}$
$\omega$	-4.1145	0.6695		$6.21 \bullet 10^{-1}$		0.0117	<b>0.9998</b>	-0.0020
$t_c$	0.0270	$9.26 e^{-4}$	$5.38 e^{-5}$	$8.53 \bullet 10^{-7}$		$-7.62 e^{-5}$	0.0020	<b>1.0000</b>
<i>IBovespa</i>								
$t_1^* \approx \text{Jun. 2003}, t^2 \approx \text{Jan. 2004}$								
Hessian $\mathbf{H}(\phi^*)$			$\lambda$			Eigenvectors $\vec{v}$		
	$m$	$\omega$	$t_c$			$m$	$\omega$	$t_c$
$m$	2.2941			$2.29 \bullet 10^0$		<b>0.9999</b>	0.0141	0.0015
$\omega$	-0.0323	0.0108		$1.04 \bullet 10^{-2}$		0.0141	<b>0.9998</b>	0.0157
$t_c$	0.0029	$1.2 e^{-4}$	$7.2 e^{-6}$	$1.61 \bullet 10^{-6}$		0.0012	0.0157	<b>-0.9999</b>

**Table III** Hessian matrix, eigenvalues and corresponding eigenvectors for the best LPPLS fits for the four studied empirical bubbles described in section III.A using Eq (13). The numbers represented in boldface identify the parameters that contribute most to their corresponding eigenvalue.

Index	Damping	Number of oscillations	LPPLS conditions	AR(1) residuals ( $\vec{r}$ ) test	
				Dickey-Fuller	Phillips-Perron
<i>Synthetic</i> LPPLS	3.36	5.27	Satisfied	-3.420 ( $10^{-3}$ )	-3.610 ( $10^{-3}$ )
SSEC	1.04	3.91	Satisfied	-4.653 ( $10^{-3}$ )	-4.642 ( $10^{-3}$ )
<i>S&amp;P</i> 500( <i>SP</i> )	1.15	5.13	Satisfied	-4.710 ( $10^{-3}$ )	-4.702 ( $10^{-3}$ )
<i>S&amp;P</i> 500( <i>BM</i> )	1.41	4.02	Satisfied	-3.641 ( $10^{-3}$ )	-3.641 ( $10^{-3}$ )
<i>IBovespa</i>	1.85	3.47	Satisfied	-4.620 ( $10^{-3}$ )	-4.610 ( $110^{-3}$ )

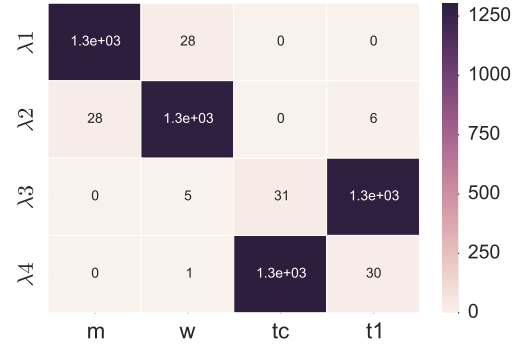
**Table IV** Diagnosis of the LPPLS fits with calibrated parameters  $\Phi^*$  for the four studied empirical bubbles described in section III.A and one synthetic data. We easily reject the hypothesis that the residuals are unit-root at the 99% confidence level. Values in brackets give the *p-values* of the test statistic.



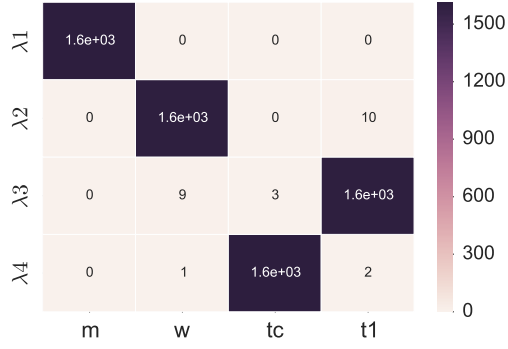
**Figure 10.** Using the original cost function (12), these 5 panels quantify the relative importance of the parameters contributing to the eigenvalues  $\lambda_1, \lambda_2$  and  $\lambda_3$  of the Hessian matrix  $\mathbf{H}(\phi^*)$  of the 4 empirical bubbles plus one synthetic bubble as discussed in the text for a given  $\bar{t}_2$  and by scanning  $t_1$ . As an example, consider the upper right panel (a) for the  $SSEC$  bubble. The upper left box with the number  $5.8 \cdot 10^2$  indicates that 580 time windows (out of the total of 580 time windows obtained by scanning  $t_1$ ) had the eigenvector associated with the largest eigenvalue  $\lambda_1$  dominated by parameter  $m$ . We also read that only one window showed parameter  $tc$  dominating the second eigenvalue  $\lambda_2$ , while  $w$  was most often the dominating parameter. Panel (d) shows that, for the  $I Bovespa$  bubble, the eigenvector associated with the largest eigenvalue was mostly dominated by parameter  $m$  (for about 380 windows) but 79 windows had parameter  $w$  as the leading parameter. The colours associated with each box convey the same information, with the color code given on the right of each table of each bubble.



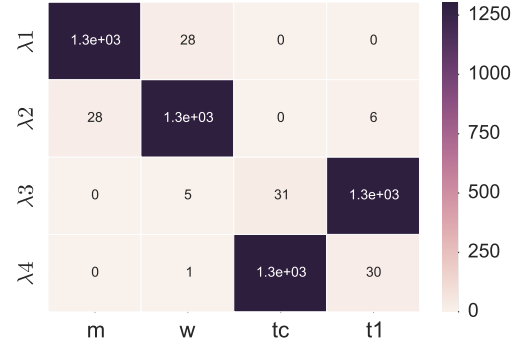
(a) *SSEC*



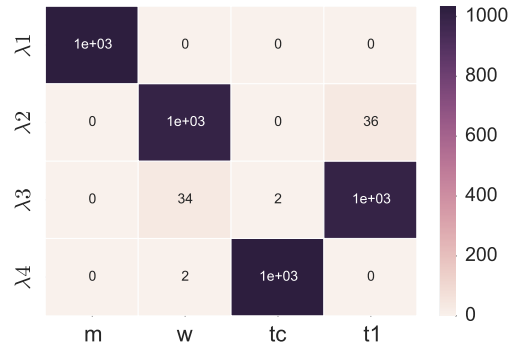
(b) *S&P500 (SP)*



(c) *S&P500 (BM)*



(d) *IBovespa*



(e) *LPPLS*

**Figure 11.** Same as figure 10 but using the extended cost function (4).